Paragliders as probes of the Alpine boundary layer: sink polars from 86 000 flight logs and the flow field of a valley

Jörg Korner

Independent researcher, Switzerland
joergkorner@gmail.com
ORCID: https://orcid.org/0009-0001-9201-7509

Preprint statement

This manuscript is a non-peer reviewed preprint submitted to EarthArXiv.

The manuscript is not under consideration by a journal at the time of this submission.

Revised version of 15 October 2026. The first version (7 October 2026, under the title "Separating the glider from the air: paraglider sink polars and the flow field of an Alpine valley from 86 000 flight logs") is available at https://joerxc.org; this version adds the correction for the choice of speed within the measured window, determined with the air seen by neighbouring pilots and iterated until the polars used for the neighbours are the polars obtained (Section 3.7), and a table of polars in which every value lies inside the measured window.

Licence

CC BY 4.0 (Creative Commons Attribution).

Data availability

The flight logs were provided by XContest and are not public; pilot names were replaced by an anonymous key to count pilots per glider type and are neither stored nor published. The segmentation and histogram code is openly available (`flightstates` 2.2, `polarmaker` 1.4). The polars of Appendix D are available in machine-readable form at https://joerxc.org/Korner_2026_polars.csv.

Paragliders as probes of the Alpine boundary layer: sink polars from 86 000 flight logs and the flow field of a valley

Jörg Korner
Independent researcher, Switzerland
joergkorner@gmail.com

Revised, 15 October 2026

Abstract

Paraglider flight logs are a dense, free and continuous record of the air over mountains: every thermal day, hundreds of pilots fly for hours along the slopes and across the valleys and record their vertical speed once per second. The obstacle is that a vario measures the air plus the sink of the glider, and the sink polars of paragliders are unknown. We obtain them from the logs themselves. Pilots choose their speed by the air: they slow down in lift and push full speed in strong sink and when leaving a thermal. But at some airspeeds, the ones they fly most, glider and pilot together are nearly a constant and only the air varies, so the most frequent vertical speed in straight flight there is the sink of the glider. The physical form of the polar shows where this holds: in a window around the airspeeds flown most, the measured points follow the physical curve; outside it they do not, and the logs show that these points lie in special air. We show this for each class of gliders and use only the window. What the choice of speed still carries into the window is measured with the air found by neighbouring pilots, whose airspeeds do not depend on the airspeed of the glide, and removed. Polars for 73 glider types follow, precise to $\pm 0.03\,\mathrm{m\,s^{-1}}$ at the airspeeds flown most, enough to see a new race harness arrive, and to find the same polar for one wing in two cloths. With the polars removed, 2.0 million glides from 86 190 flights in the Valais, 2007–2026, 153 million seconds of straight flight in all, become measurements of the air and yield a flow field of the whole valley system on a 0.5 km grid, by height and hour of day, which shows the slope and valley circulation and holds in years not used to build it. It measures what climbs cannot: the air between the thermals, free of the glider and pilot effects that climb rates carry.

1 Introduction

Every day with thermals, hundreds of paragliders fly for hours through the convective boundary layer of the Alps and record where they went and how fast they rose and sank. These flight logs are a measurement platform for the air over mountains that no instrument network matches in density, provided that the glider can be separated from the air. Thermal convection in the boundary layer is otherwise observed by radiosondes, research aircraft and remote sensing, and, increasingly, by animals and people who use it: soaring birds have served as probes of updrafts for decades (Shannon et al., 2002; Treep et al., 2016), and the flight logs of paraglider pilots have been used to compare human and bird soaring strategies (Ákos et al., 2008). Recently, Hernández-Aguayo et al. (2026) assembled 1.47 million climbing segments from 110 730 paraglider flights over France and related three climb observables (thermal ceiling, mean climb rate and its variability) to 120 predictors from the ERA5 reanalysis, aggregated to reanalysis grid cells of

0.25° and one hour. Their flight phases are detected with the method of Vilpellet et al. (2026), which distinguishes search, climb and transition; the analysis of Hernández-Aguayo et al. (2026) uses the climbing phases only.

A variometer does not measure the air. It measures the vertical speed of the glider, which is the vertical velocity of the air plus the sink of the glider through the air. The second term depends on the glider and its airspeed; the curve that describes it is the sink polar. Hernández-Aguayo et al. (2026) write the climb rate as the thermal updraft minus a glider sink of about 1.0–1.2 $\mathrm{m\,s^{-1}}$ common to all gliders. This is a fair approximation for a climatology of climbs, but it does not separate glider and air, and it leaves the glides unused: the long straight stretches between thermals, where the air between the updrafts can be observed. To read the air from a glide, the sink of the glider at the airspeed flown has to be known to a few hundredths of a metre per second.

For paragliders such polars are generally not available. Certification according to EN 926-2 classifies gliders by their flight safety characteristics, not by their performance, and manufacturers rarely publish sink polars. Methods to determine polars in flight exist for sailplanes (Marsden, 1985; Wagner, 1994) and have been applied to a paraglider with dedicated instruments (Teskey et al., 2006); wind-tunnel and flight tests address the aerodynamics of paraglider wings (Babinsky, 1999; Kulhánek, 2019) and wind-tunnel tests and simulations that of pilot fairings (Berthus, 2024). To our knowledge, sink polars have not yet been derived from large sets of ordinary flight logs.

This paper does two things. First, it describes a method that measures the sink polar of every glider type with enough recorded flights, from nothing but those flights, and applies it to 73 types (Sections 2–4; all polars are listed and drawn in Appendix D). It rests on one observation about how pilots use speed: at some airspeeds, those flown most, glider and pilot are nearly a constant and only the air varies. The physical form of the polar shows, for each class of gliders, in which window of airspeeds this holds, and the method uses no glide outside it; what the choice of speed still carries into the window is measured with the air found by neighbouring pilots, whose airspeeds do not depend on the airspeed of the glide, and removed, in a loop until the polars used for the neighbours are the polars obtained (Section 3.7). As tests of its resolution we use two natural experiments: a change of harness among the pilots of one competition glider, which must show, and one wing sold in two cloths, which must not. Second, it uses the polars to build a flow field of the Valais: the vertical velocity of the air along the glides, resolved in space, height and time of day, and tested on years not used to build it (Section 5). The flow field is a climatological mean; the thermals, which it does not contain, are shown from the climbs at one example place. Section 6 shows what climb rates contain besides the air, in relation to Hernández-Aguayo et al. (2026), and Section 7 discusses the limitations.

2 Data

2.1 Flight logs and segmentation

XContest, an online cross-country contest to which pilots upload their flight logs (XContest, 2026), provided for this study 86 369 IGC flight logs from the Valais, recorded between 2007 and 2026, of which 86 190 could be read. A log stores position and altitude, in most cases once per second, and a free-text glider name in its header. Pilot names were not used.

Each log was processed by the segmenter `flightstates` (version 2.2) and the histogram code `polarmaker` (version 1.4) (Korner, 2026). The log is resampled to 1 s. A second counts as circling if the heading changes by more than 60° within a centred 20 s window; on hand-marked flights this rule agreed with the manual classification for 94.7 % of the seconds. The wind is taken from the drift of each circling phase of at least 1.5 turns and 30 s, and interpolated in

time between circling phases. The airspeed of a straight second is the ground velocity minus this wind. Straight flight is cut into segments where the recorded vertical speed or the ground track changes. `polarmaker` stores, for every flight, histograms of the vertical speed of straight seconds in airspeed bands centred on 25, 30, . . . , 65 km h^{-1}, after rescaling to a reference altitude (Section 3.2); for the polars the same histograms are computed from the logs in bands 1 km h^{-1} wide, from 25 to 62 km h^{-1}.

2.2 Thermal strength of the day

For every flight with at least 5 min of circling and 5 min of straight flight (77 570 flights) we compute the mean climb rate while circling, as height gained over time spent circling. The thermal strength of a day, W, is the median of these climb rates over all such flights of that day, whatever the glider; it is defined for days with at least five such flights (2 365 days, 66 083 flights). On weak days W is around 0.4 m s^{-1}, on strong days 1.3 m s^{-1}.

2.3 Glider types

Glider names are typed by pilots and come in many spellings. We map them to types with a rule table: manufacturer names, start numbers, colours and sizes are removed, spellings are merged ("alpina4" and "Alpina 4"), and a short list of explicit corrections handles typing errors. Where it is unclear whether two names denote the same wing, they are kept apart: a wrongly separated name costs a few flights, a wrongly merged one biases a polar. The original Zeolite, the Zeolite GT and the Zeolite 2 GT are therefore separate types, as are the Peak 6 and the older Icepeak 6; the first two, the same wing in two cloths, serve as a null experiment in Section 4.5. The Zeolite 2 and the Zeolite 2 GT are the same wing in different cloth and are merged. Table 1 shows how many flights remain at each step. Each type with at least 100 flights on days with known W is a candidate for a polar; there are 106 such types with 26 095 flights, and 73 of them obtain a polar (Section 3.6); 28 are excluded because their polar rests on a single pilot. The certification class of each type (EN A to D, CCC for competition gliders) was taken from the manufacturers' documents and test reports; for older wings the LTF class is converted (1-2 as B, 2 as C, 2-3 as D), and for wings certified in different classes by size or weight we use the class of the main sizes at the recommended weight.

Table 1: From flight logs to polars.

Step	Flights
Flight logs provided	86 369
readable	86 190
with at least 5 min of circling and 5 min of straight flight	77 570
on days with a thermal strength W (at least 5 such flights that day; 2 365 days)	66 083
with a glider type from the name table	39 968
in the 106 types with at least 100 flights	26 095
in the 73 types with a polar	20 586
of the 106 types, EN D class (18 types, 1 043 days)	5 096

3 Method: sink polars

The polar of a glider type is obtained in five steps, each described in its own section. Every straight second of every flight of the type is rescaled to a reference altitude (Section 3.2) and raised by the sink of the air between the thermals on its day, a correction measured from the flights (Section 3.5). The most frequent vertical speed per airspeed band is the sink of the glider where glider and pilot are a constant (Sections 3.3 and 3.4); the window of airspeeds in which this holds is found from the data for each class (Section 3.6). What the pilots' choice of speed still carries into the window is measured with the air found by neighbouring pilots, whose airspeeds do not depend on the airspeed of the glide, and removed by a tilt of the band values, the second correction measured from the flights, in a loop until the polars used for the neighbours are the polars obtained (Section 3.7). The physical form of the polar is then fitted to the corrected band values inside the window (Section 3.6), and every interval comes from resampling flights (Section 3.8).

3.1 One equation per second

In a second of straight flight the recorded vertical speed $\dot{z}$ is

$$\dot{z} = w + s_g(v), \tag{1}$$

where w is the vertical velocity of the air, v the airspeed and $s_g(v) < 0$ the sink of glider type g in still air, its polar. In any single second w is unknown, so equation (1) cannot be solved for s_g. It can be solved statistically, because at the airspeeds that pilots fly most, glider and pilot are the same in every second flown at the same airspeed, whereas w differs from second to second; Section 3.3 says where this holds, and Section 3.7 measures and removes what remains of the pilot's choice within that range.

3.2 Density

In thinner air a glider at the same angle of attack flies faster and sinks faster, both by the factor φ^{-1} with

$$\varphi(h) = \sqrt{\rho(h)/\rho(h_0)}, \tag{2}$$

where ρ is the density of the ICAO standard atmosphere (Int, 1993) at the pressure altitude h of the recorder and $h_0 = 2000\,\mathrm{m}$ is the reference altitude. Every second is rescaled, $v_0 = \varphi v$ and $\dot{z}_0 = \varphi \dot{z}$, before it is counted. Between 1000 and 3000 m the factor changes the sink by about 10 %. All polars in this paper refer to 2000 m.

3.3 How pilots use speed

Equation (1) can be solved statistically only if, at a given airspeed, most seconds are flown in air whose vertical velocity does not depend on the choice of that airspeed. Pilots, however, choose their speed according to the air (MacCready, 1958): they slow down in rising air and speed up in sinking air. The method therefore rests on an assumption about this choice: at the airspeeds that the pilots of a class fly most, with little or no speed bar, they glide through ordinary air. Clearly slower and clearly faster flight is kept for special air: pilots slow down in lift, and they fly fast to cross strong sink and while leaving a thermal, where the air still rises. Where the assumption holds, the data follow the physical form of the polar. We therefore let the data decide, for each class, in which window of airspeeds it holds, and determine the polars in this window only (Section 3.6). Of the glide time of all types, 61 % lies in the window of the type, 19 % below and 20 % above it. Fast glides are rare: 6 % of the glide time is flown more than $5\,\mathrm{km\,h^{-1}}$ above the window, 9 % above $47\,\mathrm{km\,h^{-1}}$. Section 4.2 shows that the special air is visible in the data; the polars use no glide outside the window, and the flow field hardly changes without the glides above it (Section 5.4). Within the window the assumption holds only approximately: pilots follow the air gradually also there. Section 3.7 measures how much of this reaches the most frequent value and corrects the polars for it.

3.4 The most frequent value

For each glider type and airspeed band k ($1\,\mathrm{km\,h^{-1}}$ wide, centred on $v_k = 25, 26, \ldots, 62\,\mathrm{km\,h^{-1}}$) we take the most frequent value of $\dot{z}_0$ over all straight seconds of all flights of that type,

$$m_g(v_k) = \mathrm{mode}\{\dot{z}_{0,i} : |v_{0,i} - v_k| < 0.5\,\mathrm{km\,h^{-1}}\}, \tag{3}$$

from a histogram with $0.05\,\mathrm{m\,s^{-1}}$ bins, smoothed over five bins and refined by a parabola through the peak. For tables and figures we also use bands $5\,\mathrm{km\,h^{-1}}$ wide, centred on 35, 40, …, $60\,\mathrm{km\,h^{-1}}$.

Figure 1 shows why the mode and not the mean is used. The distribution of the vertical speed at $45\,\mathrm{km\,h^{-1}}$ for the EN D class has a sharp peak and a long tail towards rising air. Mean and median are pulled into the tail, by an amount that differs between airspeeds, because the air a pilot meets depends on how fast he chooses to fly (MacCready, 1958); they describe the pilots' choices as much as the glider. The mode stays where most seconds are. As a control we use the seconds in which the vario was steady for a full minute and no circling occurred within two minutes, selected without looking at the value of the vario. Their mode lies within $0.01\,\mathrm{m\,s^{-1}}$ of the mode of all seconds (Figure 1).

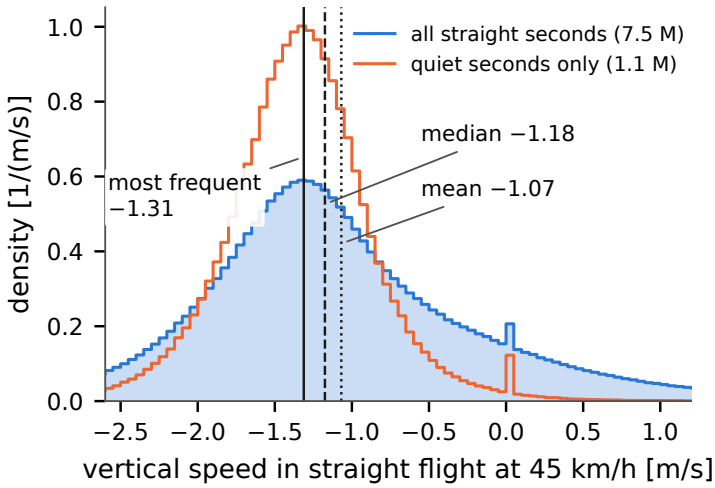

Figure 1: Distribution of the vertical speed in straight flight at $45 \pm 2.5\,\mathrm{km\,h^{-1}}$ for the EN D class (5 096 flights, rescaled to 2000 m, before the subsidence correction). Blue: all 7.5 million straight seconds; orange: the 1.1 million quiet seconds (steady vario for one minute, no circling within two minutes). The most frequent value is $-1.31\,\mathrm{m\,s^{-1}}$ for all seconds and $-1.32\,\mathrm{m\,s^{-1}}$ for the quiet ones; the median (-1.18) and the mean (-1.07) are pulled towards rising air. The spike at $0\,\mathrm{m\,s^{-1}}$ comes from seconds with unchanged recorded altitude.

3.5 The air between the thermals sinks

The mode in equation (3) is the sink of the glider in the air where most glide seconds are spent, and that air is not still. What rises in the thermals must sink elsewhere. If thermals cover a fraction f of the area and rise at a speed measured by W (Section 3.9 discusses this), mass continuity requires the remaining air to sink on average at

$$\bar{w}_{\mathrm{env}} = -\frac{f}{1-f}\,W. \tag{4}$$

Pilots, however, do not glide through the sky at random; they choose their lines, and the seconds we count are the seconds they chose. The sink in the air they glide through need not equal $\bar{w}_{\mathrm{env}}$. What equation (4) suggests is the form, a sink proportional to W. We therefore write the mode on a day of thermal strength W as

$$m_g(v_k; W) = s_g(v_k) - c\,W, \tag{5}$$

with a coefficient c that the flights must determine, and check whether the proportionality holds.

The two unknowns differ in nature. s_g belongs to the glider and is fixed by the position of the peak, which the seconds of one type determine well. c belongs to the air and is seen only across days, because all seconds of a day share one W; the total shift from the weakest to the strongest days is about $0.15\,\mathrm{m\,s^{-1}}$, comparable to the uncertainty of a single type on a single day. We therefore determine c once, from the 18 types of the EN D class, a large group of gliders of similar performance, and then the polar of every type with c fixed.

For each EN D type g and each class j of days (W in 0–0.6, 0.6–0.8, 0.8–1.0, 1.0–1.2, 1.2–1.5 $\mathrm{m\,s^{-1}}$), we compute the deviation $\delta_{g,j}(v_k) = m_{g,j}(v_k) - m_g(v_k)$ of the mode on those days from the mode of the same type on all days. Comparing each type only with itself removes the differences between gliders. The deviations are averaged over the types, weighted by the number of flights in each cell (the variance of the mode of a cell with n flights decreases roughly as $1/n$), and a straight line in W with a common slope and one intercept per group is fitted to

three groups of the 1 km h^{-1} bands, 35–38, 39–41 and 42–45 km h^{-1}, weighted by the inverse variance of the class means. Intervals come from resampling the types.

Figure 2 shows the result. The points lie on straight lines: on weak days ($W = 0.35\,\mathrm{m\,s^{-1}}$) the gliders appear to sink 0.03–0.05 m s^{-1} less than on average, on the strongest days ($W = 1.29\,\mathrm{m\,s^{-1}}$) 0.08–0.12 m s^{-1} more. The common slope is $c = 0.118$ (95 %: 0.080–0.137). The slopes of the three groups, 0.094 (0.028–0.120), 0.130 (0.081–0.155) and 0.137 (0.106–0.169), agree within their intervals, as they must if the shift is sinking air, which carries a glider down by the same amount at every airspeed. Determined from one type alone, c ranges from -0.03 to 0.24, which is why it is taken from the class.

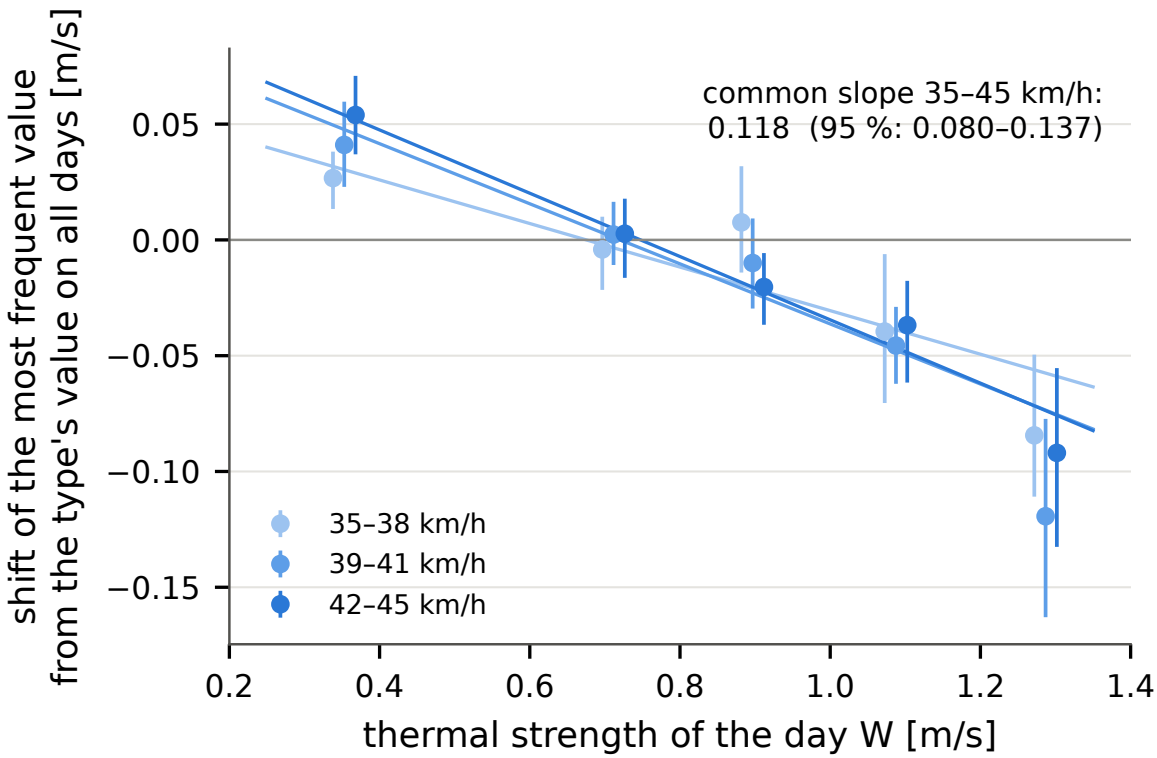

Figure 2: Shift of the most frequent value with the thermal strength of the day, EN D class (18 types), for three groups of airspeed bands. Each point is the flight-weighted mean over the types of the deviation from the type's mode on all days, at the mean W of its class of days; bars are 95 % intervals from resampling types; lines have the common slope $c = 0.118$.

Read as a mass balance, with W taken as a measure of the updraft speed, $c = f/(1-f) = 0.118$ would correspond to thermals covering 11 % of the area, of the size found for thermal plumes in large-eddy simulations and observations of the convective boundary layer, 0.1–0.2 (Couvreux et al., 2010). We do not interpret c this way, because it measures the sink in the air the pilots chose, not the mean over the sky. For the polar the distinction does not matter: the polar is counted from the same chosen seconds, and what must be removed from them is the sink in those seconds, which is what c measures.

Every straight second of a flight is therefore raised by $c\,W$ of its day before it is counted. A flight on a day with $W = 0.7\,\mathrm{m\,s^{-1}}$ gains $0.08\,\mathrm{m\,s^{-1}}$, one on a day with $W = 1.3\,\mathrm{m\,s^{-1}}$ gains $0.15\,\mathrm{m\,s^{-1}}$. The result is the polar extrapolated to $W = 0$, which we call the polar in still air; Section 3.9 discusses what this limit means.

3.6 The physical curve

For a wing at constant loading, a parabolic drag polar $C_D = C_{D0} + KC_L^2$ (Anderson, 2016) gives the sink

$$s(v) = a\,v^3 + \frac{b}{v}, \qquad a = -\frac{\rho S C_{D0}}{2mg}, \quad b = -\frac{2Kmg}{\rho S}, \tag{6}$$

with v in $\mathrm{m\,s^{-1}}$, S the wing area, m the total mass and g the gravitational acceleration. The first term is the drag of glider and pilot, the second the drag due to lift. We fit a and b by weighted least squares to the modes in the $1\,\mathrm{km\,h^{-1}}$ bands of a window of airspeeds, after the two corrections of Sections 3.5 and 3.7. Each band is weighted with the inverse variance of its mode, from resampling flights (Section 3.8) combined with $0.01\,\mathrm{m\,s^{-1}}$ for the resolution of the mode, and is used if it holds at least 3 000 seconds.

The window is found from the data, once for each class. It starts at the most flown airspeed of the class, $\pm 3\,\mathrm{km\,h^{-1}}$, and grows band by band, downwards and upwards, as long as the new band lies within two standard errors of the curve fitted without it and χ^2 of the whole window stays below its 95 % limit. It starts there because that is where the assumption of Section 3.3 places the ordinary air; the points in special air may also lie on a smooth curve. The windows are 29–37 $\mathrm{km\,h^{-1}}$ for EN A (most flown airspeed $34\,\mathrm{km\,h^{-1}}$), 32–40 $\mathrm{km\,h^{-1}}$ for EN B (36) and EN C (37), 34–48 $\mathrm{km\,h^{-1}}$ for EN D (39) and 34–51 $\mathrm{km\,h^{-1}}$ for the competition class (41). Figure 3 shows them with the points of each class. A type is given the window of its class, shifted by the difference between its own most flown airspeed and that of its class, rounded to $1\,\mathrm{km\,h^{-1}}$. It obtains a polar if at least eight bands of its window around its most flown airspeed are usable and χ^2 stays below the 95 % limit. This holds for 101 of the 106 types; for four the points do not follow the physical curve within the window, and one has too few seconds (Appendix D). A third condition concerns the pilots. A polar measured from few pilots is the polar of those pilots, with their weight, their harness and their way of flying, and the intervals from resampling flights do not show it. The flight logs name the pilot in their header; we replace the name by an anonymous key and never store it, and for every type we also fit the polar without the pilot who flew the most flights of that type. The pilot with the most flights of a type has 20 % of them in the median; for 34 types he has less than 15 % and leaving him out changes the polar by $0.005\,\mathrm{m\,s^{-1}}$ in the median, for 41 types he has 15–30 % ($0.008\,\mathrm{m\,s^{-1}}$), and for 25 types 30 % or more ($0.018\,\mathrm{m\,s^{-1}}$ in the median, up to 0.09). A type obtains no polar in two cases. Where the pilot with the most flights has 30 % of them or more, the other flights cannot establish the polar on their own, and the comparison without him proves nothing: 25 types, with one pilot flying 30–70 % of the logs. Where leaving him out changes the polar by more than $0.03\,\mathrm{m\,s^{-1}}$ at the most flown airspeed or $0.05\,\mathrm{m\,s^{-1}}$ at the end of the window, roughly the 95 % interval of a type, the polar is his and not the glider's: three further types. The 28 types are listed in Appendix D with the share of that pilot; 20 of them are EN A and B types, which the pilots of a cross-country database fly in small numbers. Among the excluded EN D types is one whose most frequent pilot sinks $0.18\,\mathrm{m\,s^{-1}}$ less than the other pilots at the fast end of the window and the same at its slow end, the signature of a faired harness (Section 4.4). The remaining 73 types have their polars in Appendix D. Of their 738 band values, 99.1 % lie within their 95 % interval of the fitted curve, and the median of χ^2 per degree of freedom over the types is 0.79. Within the window the curve is a fit to measurements; outside, it is the extension of the physical form. How much of its shape the measurements fix depends on the width of the window. Once the sink s and its slope s' at one airspeed are given, equation (6) fixes the bending, $v^2 s'' = 3s + vs'$. In the narrow windows of the EN A, B and C classes the points determine the level and the slope of the polar around the most flown airspeed; its bending, and with it the airspeed of the best glide ratio and the extension, come from the physical form. In all classes the points lie slightly flatter than the curve: relative to the curve, they are higher at the ends of the window than in its middle, by 0.01–0.015 $\mathrm{m\,s^{-1}}$ and for EN A by $0.03\,\mathrm{m\,s^{-1}}$ (Figure 3). In the narrow windows this

is nearly the whole bending of the curve, and the points of the EN A, B and C classes lie almost on a straight line (Section 7). How far the physical form carries beyond a narrow window can be measured in the classes with wide windows: fitted to a window as narrow as that of EN B, the curve of the EN D class predicts the measured bands up to 5 km h^{-1} beyond it to within 0.01–0.03 m s^{-1} (Appendix C). From equation (6), the best glide ratio is reached at $v^* = (b/a)^{1/4}$ and the minimum sink at $(b/3a)^{1/4}$; both may lie outside the window.

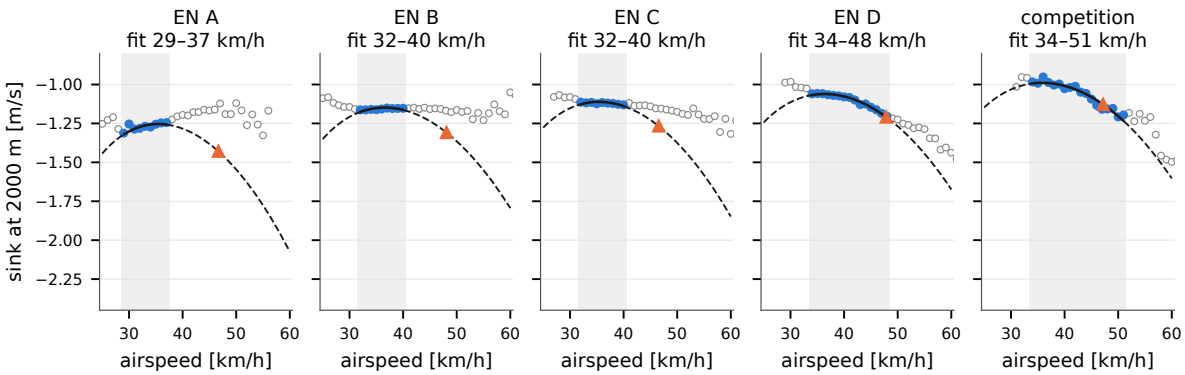

Figure 3: Polars of the five classes, all types of a class together, at 2000 m. Points: most frequent value in 1 km h^{-1} bands after the corrections for subsidence and for the choice of speed; filled in the window (shaded), open outside. Line: the physical curve fitted in the window, dashed outside. Triangle: best glide ratio of the curve. Outside the window the points lie above the curve, the gliders appear to sink less (Section 4.2).

3.7 The choice of speed within the window

Fitted to the modes of Section 3.4 with the day correction alone, the polars are provisional. The most frequent value is the sink of the glider only if the air in which a pilot flies at a given airspeed is ordinary air, not chosen; but pilots choose their speed by the air, slow where it rises and fast where it sinks. The window removes the coarse part of this, the airspeeds flown only in special air. Within the window a rest remains: the air at the slow airspeeds is on average a little better than ordinary, the air at the fast airspeeds a little worse, the mode takes up part of it, and the provisional polar comes out a little too steep, too good at slow airspeeds and too poor at fast ones.

To remove this rest we need the air in which each glide was flown, from a measurement that does not use the vario of that glide, which contains the sink we are looking for. The other pilots gliding at the same place and time provide it: for them too the sink is known, from the provisional polar of their type, and their vario minus their sink is the air, the air in which our pilot flies as well. These neighbours (other flights on the same day in the same cell, height band and time span, flying at 35–43 km h^{-1}) fly at their own airspeeds for their own reasons, so what they report does not depend on the airspeed of the glide. Figure 4a shows what they report for the EN D class, against the airspeed of the glide: where a pilot glides at 34 km h^{-1}, the neighbours within 1 km find air 0.15 m s^{-1} better than the mean of the window, where he glides at 48 km h^{-1}, 0.13 m s^{-1} worse, in between nearly a straight line, 0.18 m s^{-1} per 10 km h^{-1}. The closer the neighbours, the more of the air at the glide they share, and the steeper the line: 0.09 m s^{-1} per 10 km h^{-1} within 2 km, 0.26 within 500 m, 0.30 within 250 m.

How much of this reaches the mode cannot be all of it: the polars would then be nearly flat across the window and the best glide ratio would lie near full speed instead of near trim (Section 4.3). It is measured by forming the mode twice from the same glide segments, once as in Section 3.4 with the day correction cW, and once with the neighbours' air subtracted from every

glide before the most frequent value is formed. The second curve is free of the choice of speed as far as the neighbours have seen the air, and the difference of the slopes of the two physical curves is the part that the choice carries into the polar (Appendix B). Because neighbours within 1 km see only part of the air at the glide, the measurement is repeated with neighbourhoods of four sizes, from 2 km down to 250 m, and extended to a neighbourhood of zero size, where the neighbours would see all of the air (Figure 4b).

How strongly pilots follow the air within the window is not the same for all, and the windows themselves show it. For EN A, B and C the window reaches only a few $\mathrm{km\,h^{-1}}$ above trim speed: these pilots use the speed bar for special air and hardly otherwise. For EN D and the competition class it reaches far into the speed-bar range: these pilots choose their airspeed by the day, by the climb they expect in the next thermal (MacCready, 1958), and fly faster everywhere on a strong day, in ordinary air too, so that their airspeed is largely decoupled from the air at the place. The neighbours confirm it: the gradient of their air over the window is 0.15–0.18 $\mathrm{m\,s^{-1}}$ per 10 $\mathrm{km\,h^{-1}}$ for EN D and the competition class and 0.25 for EN B and C (neighbours within 1 km). The tilt is therefore measured and applied separately for the two groups of windows, the narrow ones (EN A, B and C; measured on B and C) and the wide ones (EN D and the competition class), each from its own flights.

The neighbours' sink, however, is known only from their provisional polars, which carry the very tilt that is being measured, and with provisional polars the tilt comes out too small (Appendix B says why). The correction is therefore made in a loop: the tilt is measured, the polars are tilted by it, the neighbours' air is computed again with the tilted polars and the tilt is measured again, until nothing changes (Figure 4c). With untilted polars the tilt of all classes together is 0.063 $\mathrm{m\,s^{-1}}$ per 10 $\mathrm{km\,h^{-1}}$; with polars tilted by this amount it is 0.123; with polars tilted by 0.123 it is 0.115. The loop converges where the measured tilt equals the assumed one, and there the polars and the air they give at the neighbours agree, and nothing depends any more on where the loop started. For the two groups the self-consistent values are 0.123 $\mathrm{m\,s^{-1}}$ per 10 $\mathrm{km\,h^{-1}}$ (95 %: 0.021–0.273) for the narrow windows and 0.115 $\mathrm{m\,s^{-1}}$ per 10 $\mathrm{km\,h^{-1}}$ (0.020–0.257) for the wide ones: the same within their uncertainty. The mode thus absorbs about a third of the air gradient that the neighbours see at zero size, 0.32 $\mathrm{m\,s^{-1}}$ per 10 $\mathrm{km\,h^{-1}}$ (Appendix B); the large-scale part of the air that pilots follow enters it, the small-scale part, the thermals and sink that pilots react to most, lies in the tails of the distribution and leaves its peak alone. In the terms of Figure 1: the air that pilots follow moves the mean of the distribution by up to 0.3 $\mathrm{m\,s^{-1}}$ per 10 $\mathrm{km\,h^{-1}}$ of airspeed, and its peak by 0.12.

Every polar is corrected for this before the curve is fitted: the mode of a band is raised by 0.0123 $\mathrm{m\,s^{-1}}$ (narrow windows) or 0.0115 $\mathrm{m\,s^{-1}}$ (wide windows) for every 1 $\mathrm{km\,h^{-1}}$ that the band lies above the most flown airspeed of the type and lowered by the same amount below it, a tilt about the most flown airspeed, where the neighbours' air equals the window mean and the level is not affected. Only the polars corrected in this way are called polars in the rest of this paper. The uncertainty of each group's tilt is carried into every interval (Section 3.8); comparisons between gliders of the same group, the harness experiment of Section 4.4 and the differences of the flow field are not affected by it. At the ends of the EN D window, 7 $\mathrm{km\,h^{-1}}$ from the middle, the correction is $\pm 0.08\,\mathrm{m\,s^{-1}}$, at the ends of the EN B window $\pm 0.05\,\mathrm{m\,s^{-1}}$; compared with the provisional polars it raises the best glide ratio of a type by 0.9 on average and moves it 5 $\mathrm{km\,h^{-1}}$ towards higher airspeed, which for the narrow windows lies beyond the window, on the extension of the physical curve (Section 7).

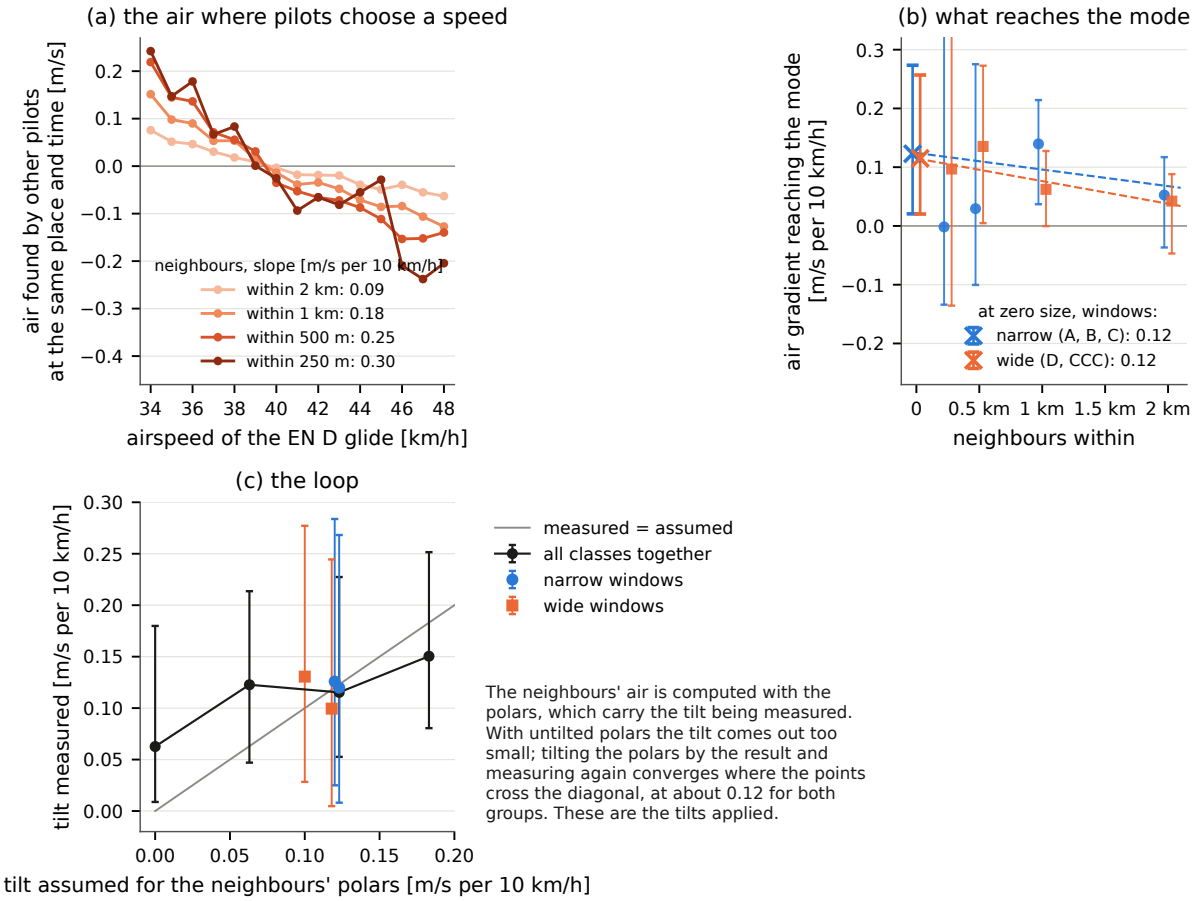

Figure 4: The choice of speed within the window. (a) The air found by other pilots at the place and time of a glide of the EN D class, against the airspeed of that glide, relative to the mean over the window: neighbours within 2 km, 1 km, 500 m and 250 m (cell s km, height band 300s m, time span 10s min; the neighbours fly at 35–43 km h^{-1} whatever the airspeed of the glide). The legend gives the slope of a straight line through the points; the 95 % intervals of the points from resampling flights are about ± 0.01 m s^{-1} within 2 km, ± 0.02 within 1 km, ± 0.04 within 500 m and ± 0.08 within 250 m. (b) How much of this reaches the most frequent value: change of the slope of the physical curve when the neighbours' air is subtracted instead of the day correction, for the four neighbourhood sizes and the two groups of windows, at the end of the loop of panel (c); dashed: weighted lines; crosses: their values at zero size, the tilts applied. 95 % intervals from 200 resamplings of the flights, the same for all sizes. (c) The loop: the tilt measured against the tilt assumed for the polars with which the neighbours' air is computed; black: all classes together, from untilted polars onwards; blue and orange: the two groups in the last two rounds. Where the points cross the diagonal, the polars used for the neighbours are the polars obtained.

3.8 Uncertainty

Seconds within one flight share the air, the trim, the pilot and the wind error and are strongly correlated; resampling seconds would give intervals that are far too narrow. The resampling unit is therefore the flight: flights are drawn with replacement, their histograms summed, the modes and the curve recomputed, 300 times. In each repetition the tilt of Section 3.7 is drawn from its own resampling distribution, one draw for both groups of windows and the same value for all types of a group, so that the intervals of a single polar contain the uncertainty of the tilt while differences between types, periods and classes of the same group do not. All 95 % intervals for polars in this paper are percentiles of these repetitions. Near the most flown airspeed they are statistical; towards the ends of a window the uncertainty of the tilt dominates, and there the intervals are asymmetric, like the distribution of the tilt.

3.9 The absolute level

The limit $W = 0$ of equation (5) is not a day we observe. W is the climb rate of circling gliders, that is, the updraft speed minus the sink of a glider in circling flight, about $1\,\mathrm{m\,s^{-1}}$. If the subsidence is proportional to the updraft speed rather than to the climb rate, it does not vanish at $W = 0$ but amounts to about $c \times 1\,\mathrm{m\,s^{-1}} \approx 0.1\,\mathrm{m\,s^{-1}}$, and all polars are then too pessimistic by up to this amount. Such a constant would shift all polars equally; no comparison between gliders would change. To check the absolute level independently, we use flights without any thermal: at most 60 s of circling, less than 50 m of height gained, 4–40 min long. There are only 63 such flights with a polar (8.5 glide hours) in a cross-country data set. The mean difference between their vario and their polar is $+0.04\,\mathrm{m\,s^{-1}}$ (95 %: -0.06 to $+0.17$; median -0.02). The polars are thus consistent with these flights, and the check is compatible both with no offset and with an offset of the size just estimated; it cannot exclude a shift of up to about $0.17\,\mathrm{m\,s^{-1}}$. Glides started before 9:00, 19 of the 63 flights, may in addition be affected by cold air sinking along the slopes.

4 Results: sink polars

4.1 The EN D class

Figure 5 shows the polar of the EN D class, all 18 types together, fitted in its window from 34 to $48\,\mathrm{km\,h^{-1}}$ after the corrections for subsidence and for the choice of speed: $a = -2.57 \times 10^{-4}\,\mathrm{s^2\,m^{-2}}$, $b = -8.04\,\mathrm{m^2\,s^{-2}}$. At $45\,\mathrm{km\,h^{-1}}$ ($12.5\,\mathrm{m\,s^{-1}}$) the drag term contributes $-0.502\,\mathrm{m\,s^{-1}}$ and the induced term $-0.644\,\mathrm{m\,s^{-1}}$, together $-1.146\,\mathrm{m\,s^{-1}}$ (95 %: -1.204 to -1.064; the interval is wide and asymmetric because $45\,\mathrm{km\,h^{-1}}$ lies $6\,\mathrm{km\,h^{-1}}$ above the most flown airspeed and the uncertainty of the tilt enters). The 15 bands of the window deviate from the curve by at most $0.02\,\mathrm{m\,s^{-1}}$ ($\chi^2 = 4.2$ for 13 degrees of freedom). The best glide ratio of the curve is 11.0 at $48\,\mathrm{km\,h^{-1}}$.

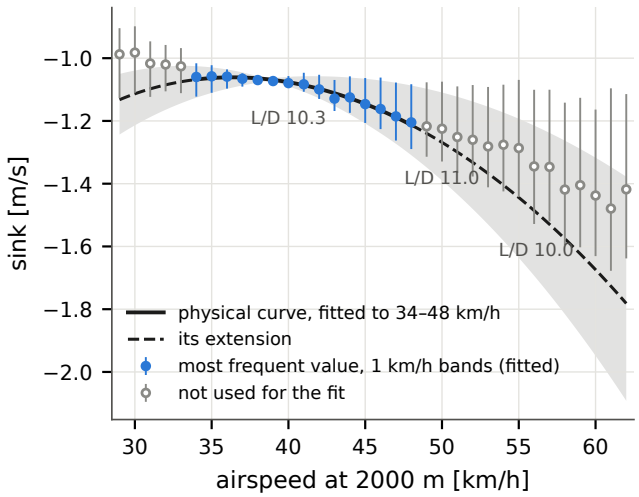

Figure 5: Polar of the EN D class (18 types, 5 096 flights, at 2000 m). Blue: most frequent value in $1\,\mathrm{km\,h^{-1}}$ bands after the corrections for subsidence and for the choice of speed, with 95 % intervals from resampling flights. Black: the physical curve fitted to the 15 bands of the window, 34–$48\,\mathrm{km\,h^{-1}}$, with its 95 % band; dashed: its extension. Open grey circles: bands outside the window; below $34\,\mathrm{km\,h^{-1}}$ and above about $49\,\mathrm{km\,h^{-1}}$ they show less sink than the curve (Section 4.2). L/D: glide ratio of the curve.

4.2 The assumption in the data

Outside the window the gliders appear to sink less than the curve predicts, in all classes and on both sides (Figures 3 and 5). Below the window this is what the assumption expects: pilots fly slowly where the air rises. Above it, the EN D class sinks less than its curve by 0.03 m s^{-1} at 49 km h^{-1}, 0.05 at 50, 0.17 at 55 and 0.27 m s^{-1} at 60 km h^{-1}. Taken at face value, its measured glide ratio would rise from 10.6 at 45 to 11.1 at 55 km h^{-1}, and that of the EN B class, whose window ends at 40 km h^{-1}, from 9.5 at 40 to 11.7 at 55 km h^{-1}, close to full speed. No paraglider glides better at full speed than near trim: in a flight test of an EN B wing, the Niviuk Hook 3, the best glide ratio, 9.3, was reached at 37.5 km h^{-1} (Heatwole, 2022).

Above the window, the deviation depends on where the fast seconds are flown (Figure 6; for this test each subset of the EN D class has its own curve, fitted to 35–45 km h^{-1}, within the window). It is largest in the first minute after leaving a thermal, +0.23 m s^{-1} at 51–55 km h^{-1} (95 %: 0.12–0.28), and much smaller more than five minutes from any thermal, +0.06 m s^{-1} (−0.01 to 0.16). A wing does not know how long ago its pilot left a thermal; the air does. Pilots accelerate while the air still rises. Far from thermals a smaller deviation remains above about 54 km h^{-1}.

Pilots also fly faster where the air sinks, as the speed-to-fly rule prescribes (MacCready, 1958). At the places and times where they glide above the window of their type, other pilots, gliding within the window of theirs in the same 1 km cell, 300 m height band and quarter of an hour, find air (computed as in Section 5) that is worse than where pilots glide within the window: by 0.17 m s^{-1} (95 %: 0.16–0.18) up to 5 km h^{-1} above the window, 0.24 m s^{-1} at 5–10 km h^{-1} above and 0.28 m s^{-1} further above. This acts against the observed deviation: in the most frequent value, the rising air after thermals outweighs it. Below the window the neighbours find better air, by 0.19 m s^{-1} (0.18–0.21) up to 5 km h^{-1} below, as the assumption expects. The choice of speed follows the air gradually, also within the window: where pilots glide in its lower half, the neighbours find air 0.13 m s^{-1} better than where they glide in its upper half; Section 3.7 measures what this does to the polars and corrects for it.

Errors of the airspeed, the wind and the vario do not explain the deviation (Appendix A). The seconds outside the window thus lie in special air. None of them enters the polars, and without the glides above the window the flow field hardly changes (Section 5.4).

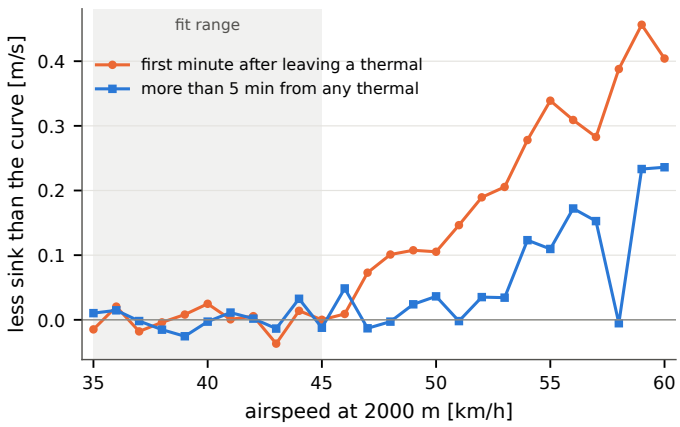

Figure 6: Less sink than the curve fitted to 35–45 km h^{-1} (shaded), EN D class, in 1 km h^{-1} bands, for seconds in the first minute after leaving a thermal and for seconds more than five minutes from any thermal; each subset has its own curve.

4.3 All glider types

Table 3 in the appendix lists the polars of all 73 types with their windows and intervals, and Figures 16 and 17 show them with the measured points. The table gives the sink at three airspeeds inside the window of each type, its start, its most flown airspeed and its end, where the curve rests on points, and the best glide ratio and the minimum sink with their intervals: the optimum of the curve where it lies inside the window, otherwise the value at the window edge, marked as a bound. At the most flown airspeed the half-width of the 95 % interval has a median of $0.02\,\mathrm{m\,s^{-1}}$, from 0.01 for the most-flown types to 0.05 at most, small against the differences between types; at the ends of the window it is 0.06 in the median, because the uncertainty of the tilt enters there. Polars with wide or very lopsided intervals are marked in the table. The classes separate as expected but overlap: weighted by flights, the sink at $35\,\mathrm{km\,h^{-1}}$ is $-1.15\,\mathrm{m\,s^{-1}}$ for the 35 EN B types, -1.12 for the 24 EN C types and -1.06 for the 12 EN D types; the only EN A type with a polar, the Koyot 3, sinks $-1.33\,\mathrm{m\,s^{-1}}$, the competition glider $-0.99\,\mathrm{m\,s^{-1}}$. Several EN C types, among them the Lyght, the Photon and the Artik R, lie close to the EN D class. The curves of the classes (Figure 3) reach their best glide ratio at 46–48 $\mathrm{km\,h^{-1}}$: 9.1 for EN A, 10.2 for EN B and EN C, 11.0 for EN D and 11.6 for the competition class. At 2000 m these airspeeds correspond to 42–44 $\mathrm{km\,h^{-1}}$ at sea-level density, a few kilometres per hour above trim speed; for the EN A, B and C classes they lie beyond the window, where the curve is the extension of the physical form.

4.4 A natural experiment: the Enzo 3 and a faired race harness

A method that measures polars from crowd-sourced flights should be able to detect a known change in a glider–pilot system. The data contain a natural experiment. The Submarine, a race harness with a full fairing around the pilot, was first flown by Ozone team pilots at a Paragliding World Cup Superfinal in 2021 (Ozone Paragliders, 2021; Wentzel, 2024); a review of the harness appeared in January 2024 (Cross Country, 2024). Ozone stated that the shape reduced drag by about 7 %, which corresponds to $0.17\,\mathrm{m\,s^{-1}}$ less sink at full speed than its previous race harness (Wentzel, 2024). Competition pilots flying the Enzo 3, Ozone's competition glider, are the most likely users. No log records the harness, so the question is whether the polar of the Enzo 3 changes, when, and in what way.

Figure 7a shows the sink of the Enzo 3 at $45\,\mathrm{km\,h^{-1}}$ year by year. 2024 and 2026 lie above all earlier years, 2025 above all except 2020. We therefore compare two periods, to 2023 (435 flights) and from 2024 (155 flights). From 2024 the measured values in bands $5\,\mathrm{km\,h^{-1}}$ wide show less sink by $+0.03\,\mathrm{m\,s^{-1}}$ at $35\,\mathrm{km\,h^{-1}}$ (95 %: -0.03 to $+0.07$), $+0.05$ at 40 ($+0.01$ to $+0.09$), $+0.09$ at 45 ($+0.03$ to $+0.14$) and $+0.09$ at $50\,\mathrm{km\,h^{-1}}$ ($+0.04$ to $+0.14$). The EN D class changes over the same periods by $+0.04$, $+0.03$, $+0.01$ and $-0.03\,\mathrm{m\,s^{-1}}$, the drift that the air, the pilots and the changing mix of gliders produce in a large group. The tilt of Section 3.7 is the same in both periods and drops out of all these differences. At 35 and $40\,\mathrm{km\,h^{-1}}$ the change of the Enzo 3 cannot be told from this drift; at 45 and $50\,\mathrm{km\,h^{-1}}$ it is several times larger, and its interval excludes zero.

A harness cannot change the wing. It can only change the drag of the pilot, which enters the term av^3 of equation (6); the induced term b/v belongs to the wing. A change of harness must therefore produce a gain that is small at trim speed and grows with speed, and it must lie in a alone. Fitting the two periods in the window of the Enzo 3, 34–51 $\mathrm{km\,h^{-1}}$, gives $\Delta a = +3.6 \times 10^{-5}\,\mathrm{s^2\,m^{-2}}$ (95 %: $+0.5$ to $+6.7 \times 10^{-5}$) and $\Delta b = -0.00\,\mathrm{m^2\,s^{-2}}$ (-0.62 to $+0.56$). The fitted curves give a gain of $0.03\,\mathrm{m\,s^{-1}}$ at $35\,\mathrm{km\,h^{-1}}$ (-0.01 to $+0.07$), $0.07\,\mathrm{m\,s^{-1}}$ at $45\,\mathrm{km\,h^{-1}}$ (0.04–0.10) and $0.10\,\mathrm{m\,s^{-1}}$ at $50\,\mathrm{km\,h^{-1}}$ (0.05–0.14), growing with speed (Figure 7b). At $45\,\mathrm{km\,h^{-1}}$ the drag term accounts for $+0.071\,\mathrm{m\,s^{-1}}$ of it and the induced term for $0.000\,\mathrm{m\,s^{-1}}$; this split was not imposed but follows from the bands of each period. The interval of Δa excludes zero;

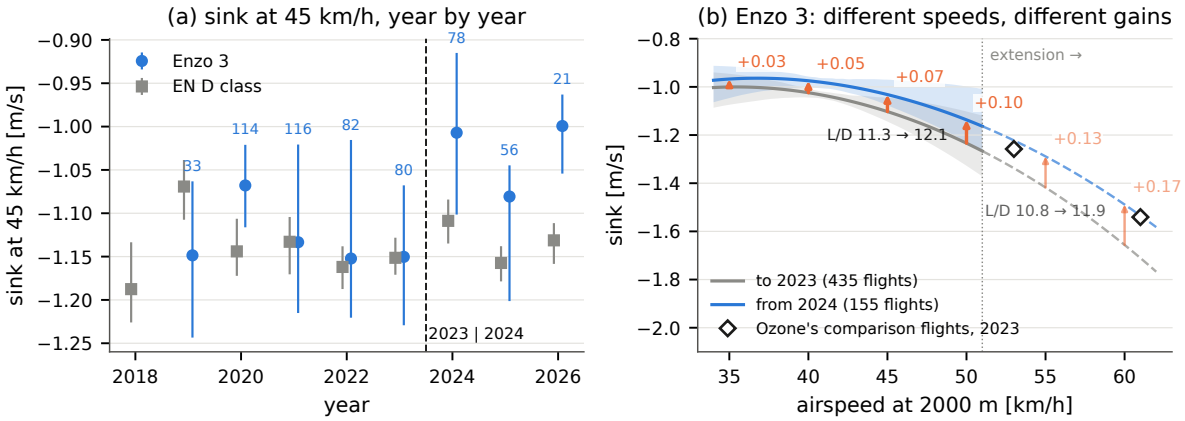

Figure 7: (a) Sink of the Enzo 3 (blue, number of flights above) and of the EN D class (grey) at 45 km h^{-1} per year, with 95 % intervals from resampling flights, without the uncertainty of the tilt, which is the same in all years and drops out of the comparison; the dashed line separates 2023 and 2024. (b) Polars of the Enzo 3 to 2023 (grey, 435 flights) and from 2024 (blue, 155 flights), fitted in the window of the Enzo 3, 34–51 km h^{-1}, with 95 % bands; dashed above 51 km h^{-1}: extension of the curves. Arrows: gain at each speed, with its value in m s^{-1}; L/D: glide ratio before and after. Diamonds: Ozone's own comparison flights of 2023 with two harnesses on the same glider, 0.08 m s^{-1} at 53 km h^{-1} and 0.17 m s^{-1} at full speed (Section 4.4), drawn as the curve to 2023 plus the gain.

that of Δb corresponds to -0.05 to $+0.05$ m s^{-1} at 45 km h^{-1}. The data thus point to a change of the drag term; a change of the induced term by a few hundredths of a metre per second cannot be excluded. A change in pilot weight would change both terms. A lower drag of the wing itself, of its lines or its profile, would produce the same signature as a harness and cannot be excluded from the data; the attribution to the harness rests on the timing and on the size of the effect. The extension of the fitted change gives $+0.17$ m s^{-1} at 60 km h^{-1} (95 %: 0.05–0.28), the size of Ozone's statement for full speed; the comparison is rough, since the reference harnesses differ and the extension is not a measurement. We attribute the change to the harness, with the reservation that this is an attribution, not an observation. Ozone's own comparison flights of August 2023 with two harnesses on the same glider show the same signature: no difference at trim speed, 0.08 m s^{-1} less sink at an indicated airspeed of 13.5 m s^{-1} (about 53 km h^{-1} at 2000 m) and 0.17 m s^{-1} at full speed (L. Armant, Ozone, personal communication, 2026). At matched airspeed the gain measured here is somewhat larger, 0.12 m s^{-1} (0.05–0.18) at 53 km h^{-1}, as expected if the harnesses flown before 2024 were on average less streamlined than the race harness of Ozone's comparison. Since not all pilots switched at the same time, the measured gain is a lower bound of the gain for a single pilot who switches.

In glide ratio, the Enzo 3 improves from 11.4 to 12.1 at 45 km h^{-1} and from 10.8 to 11.9 at 55 km h^{-1} (the latter from the extension). A single polar for the Enzo 3 would be wrong by about 0.1 m s^{-1} at speed for one of the two periods, so Appendix D gives two.

4.5 A null experiment: one wing in two cloths

The harness experiment shows that the method sees a change that must be there. The data also contain the opposite case, a change that must not show. The Zeolite (Ozone, 2019) is a lightweight wing, under 3 kg in size MS with a 27 g top cloth; the Zeolite GT is the same design built for durability, with a 38 g top cloth and a correspondingly changed internal structure, 3.7 kg, and the same handling according to the manufacturer (Cross Country, 2020). The difference of about 0.8 kg is one per cent of the flying mass. A change of mass moves a polar along a line through the origin by the square root of the load factor (Section 7), so the two polars may

differ by about 0.5 %, or 0.005 m s^{-1}, below the resolution of the method. The two types were kept apart in the name table and measured independently: 234 flights of the Zeolite (169 days, 2019–2026) and 508 of the Zeolite GT (249 days, 2020–2026), largely different pilots and days. Their polars agree to the resolution: the curves differ by 0.009 m s^{-1} at 36 km h^{-1}, 0.007 at 41 and 0.006 at 46 km h^{-1} (95 %: about ± 0.03 to ± 0.05), the best glide ratios are 10.61 at 47.2 and 10.66 at 47.0 km h^{-1}, and the measured values in the 5 km h^{-1} bands differ by 0.002 to 0.018 m s^{-1} (Table 3). Two independent sets of flights of the same wing thus give the same polar, within the intervals of Section 3.8, and a change that should not be visible is not. The successor, the Zeolite 2 GT (2024), is a different wing and has a different polar: 0.04 m s^{-1} less sink at 35 km h^{-1}, 0.01 more at 45 and 0.03 m s^{-1} more at 48 km h^{-1}.

5 The flow field of the Valais

The flow field built in this section is a climatological mean over two decades of flying days. It describes where and at which hour the air along the glides has tended to rise or sink, not the air of a particular day, and it samples the air along the paths that pilots chose (Section 5.2).

5.1 Construction

With the polars known, every glide segment becomes a measurement of the air. For a straight segment of duration Δt, height change Δh and mean airspeed v at altitude h, flown by a glider of type g,

$$w = \frac{\Delta h}{\Delta t} - \frac{s_g(\varphi v)}{\varphi}, \tag{7}$$

with $\varphi = \varphi(h)$ from equation (2) and s_g from equation (6); the polar is continued beyond its window, down to 20 and up to 65 km h^{-1}. Glides outside the window rely on this extension, 19 % of the glide time below and 20 % above; if the deviation of Section 4.2 is air, as the special situations suggest, they measure that air. Section 5.4 shows how much the results depend on them. Only flights whose type has a polar are used, and no correction for the day is applied, because the sinking air between the thermals is part of what the flow field describes. We use segments of at least 15 s with φv between 20 and 65 km h^{-1} between 1400 and 4200 m: 1.97 million segments, 37 100 glide hours, 24 949 flights on 2 426 days.

The flow field is the kernel-weighted mean (Nadaraya, 1964)

$$\bar{w}(\mathbf{x}, z, t) = \frac{\sum_s \Delta t_s \, K_{xy}(\mathbf{x} - \mathbf{x}_s) \, K_z(z - h_s) \, K_t(t - t_s) \, w_s}{\sum_s \Delta t_s \, K_{xy}(\mathbf{x} - \mathbf{x}_s) \, K_z(z - h_s) \, K_t(t - t_s)}, \tag{8}$$

on a grid of 0.5 km cells, with Gaussian kernels of standard deviation 0.75 km in the horizontal, 150 m in height and 45 min in local time, weighted by the duration of each segment. A value is shown only where the denominator, the effective number of glide seconds, is at least 90 s.

5.2 What the flow field shows

Figure 8 shows the flow field at 2500 m at 11:00 and 15:00 local time, for all days. At 11:00 the glides at this height follow the sunlit slopes, and the air along them rises almost everywhere (88 % of 4 071 cells, mean $+0.32$ m s^{-1}). At 15:00 the glides cover the whole valley system (11 040 cells). Rising air lies over the slopes and ridges and sinking air over the centre of the Rhône valley and some side valleys (10th percentile -0.18 m s^{-1}, 90th percentile $+0.53$ m s^{-1}). This is the pattern of the thermally driven cross-valley circulation, with upslope flow over heated slopes and compensating subsidence over the valley centre (Zardi and Whiteman, 2013). The

enlargement of the central Valais (Figure 9) shows this pattern at the scale of single slopes: closed contours of rising air over the slopes and spurs on both sides of the valley, and the zero line and weakly sinking air near the valley axis.

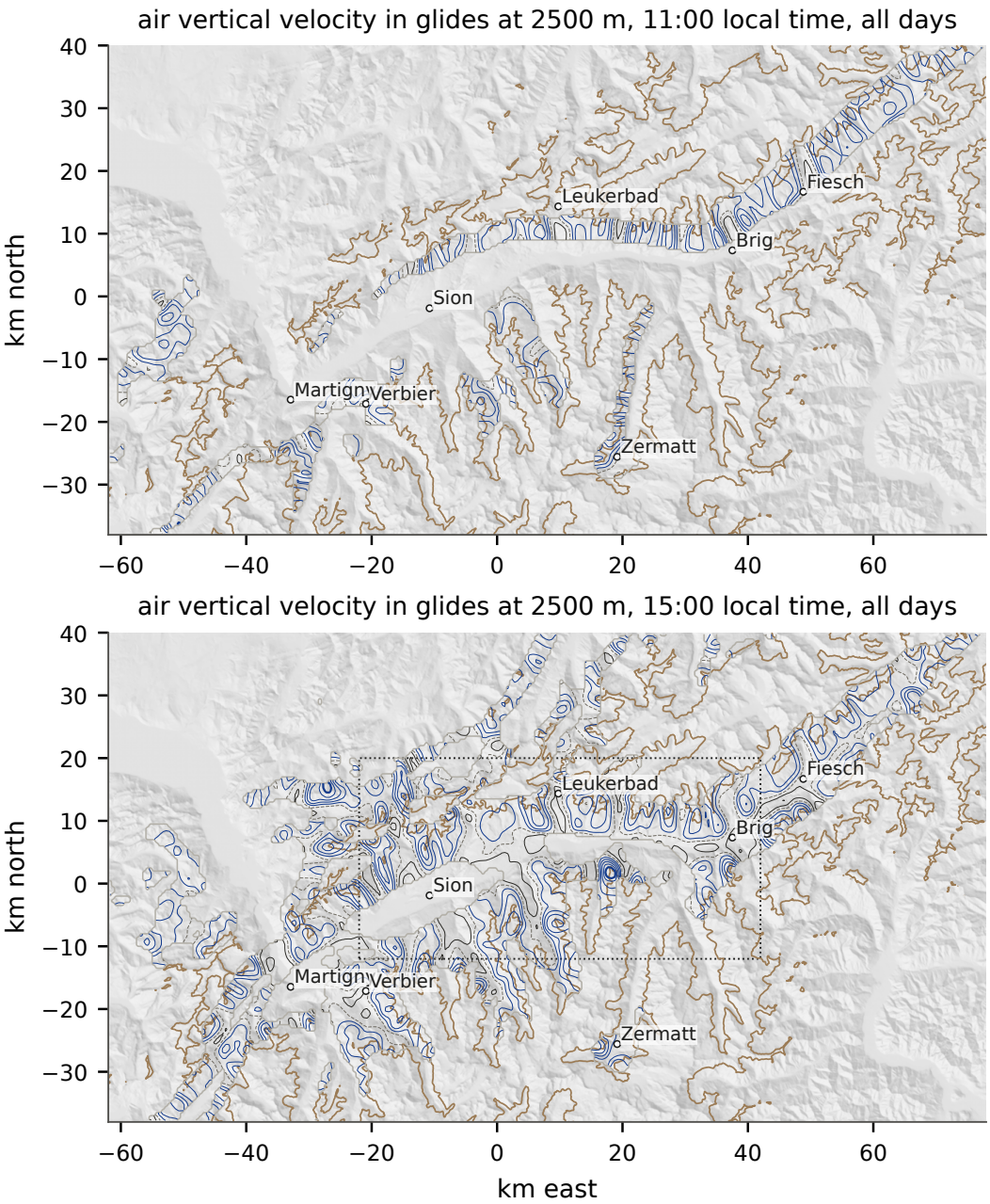

Figure 8: Flow field of the Valais: kernel-weighted mean of the air vertical velocity in glides (equation 8) at 2500 m, all days, at 11:00 (top) and 15:00 (bottom) local time. Contours every 0.2 m s^{-1}: dark blue rising, dark grey sinking, dashed zero. Light grey line: edge of the area with at least 90 effective glide seconds. Brown: the 2500 m terrain contour; shaded relief from the 3″ SRTM elevation model (Farr et al., 2007). Dotted rectangle: area of Figure 9. Coordinates in km from 46.25 °N, 7.50 °E.

The mean of the flow field is positive, +0.32 m s^{-1} over all segments, weighted by duration. This is not a violation of mass continuity, but a property of the sampling. The flow field describes the air along the paths pilots chose, and pilots seek rising air also when they do not circle: along ridges, under cloud streets, in convergence lines. The mode of the air in straight flight is close to zero or slightly negative (Section 3.5); the mean along chosen paths is not. The flow field is thus

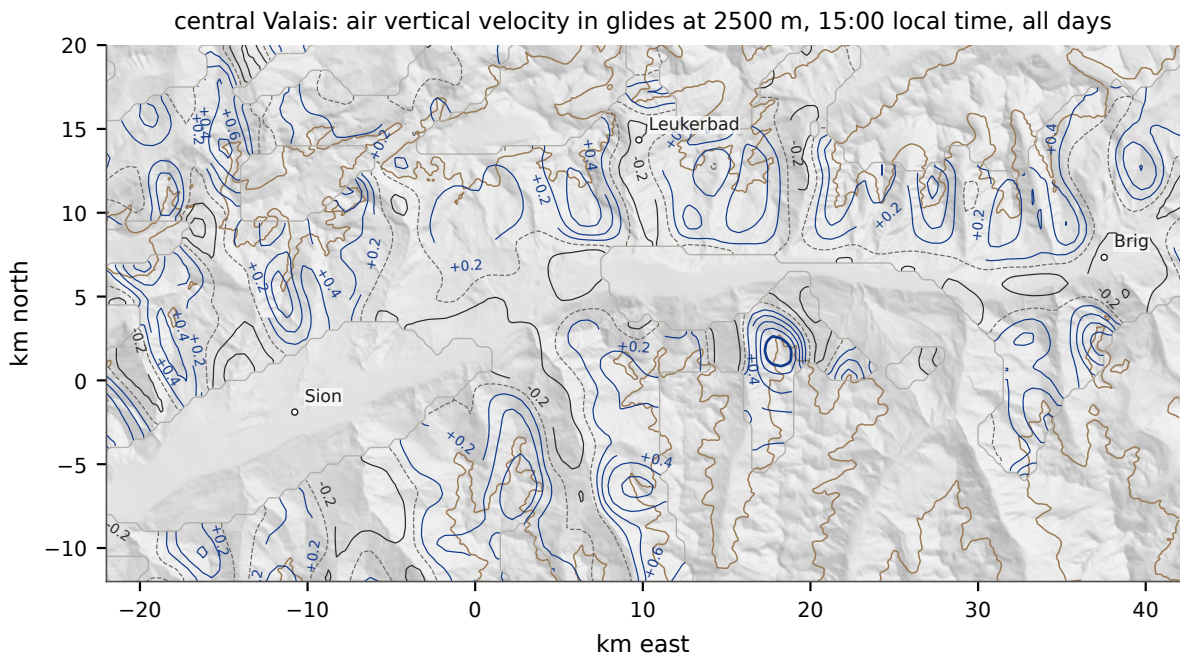

Figure 9: Central Valais, enlarged from Figure 8: air vertical velocity in glides at 2500 m, 15:00 local time, all days. Contours every 0.2 m s^{-1}, labelled in m s^{-1}; lines and relief as in Figure 8.

a map of the air available to a glider that flies like the pilots in the data set, not an areal mean of the vertical velocity. A common offset of all polars (Section 3.9) would shift it by the same amount everywhere.

5.3 The thermals

The flow field contains no circling seconds and therefore no thermal cores. To complete the picture we describe the thermals separately, from the climbs, at one example place. For each climb and 200 m height band we take the time the pilot needs to cross the band while circling, and the positions where he enters and leaves it. On a 1 km grid, per height band and hour (±1 h), all days together, this gives three quantities. The *frequency* is the fraction of pilots passing through a cell within the band who climb through it there. The *strength* is the median climb rate, corrected with the polars to the sink of the EN D class at 35 km h^{-1}, so that the glider flown does not matter; it remains the climb of an average pilot, 0.15–0.35 m s^{-1} below the best quarter (Section 6). The *drift* is the mean horizontal offset between leaving and entering the band, scaled to 1000 m of climb; it shows how the thermals lean.

Figure 10 shows the three quantities with the flow field above Fiesch, one of the most flown places of the Valais. The thermals stand on the sunlit slopes north of the Rhône, between Riederalp and the Eggishorn and above Bellwald. At 11:00 at 2500 m, 41 % of the pilots passing the slope between Fiescheralp and the Eggishorn climb there. The thermals lean up the slope: at 2500 m they drift on average 1.9 km to the north-northwest per 1000 m of climb at 11:00, 1.1 km at 14:00, and 0.5 km to the north-east, up the valley, at 17:00. Their median strength, converted to the EN D class, is 1.7–1.8 m s^{-1} at 2500 m and 2.0–2.1 m s^{-1} at 3100 m, with little change through the day; what changes is how often they are found. The air in the glides sinks over the mouth of the Fieschertal north of Fiesch, and in the afternoon also over the main valley.

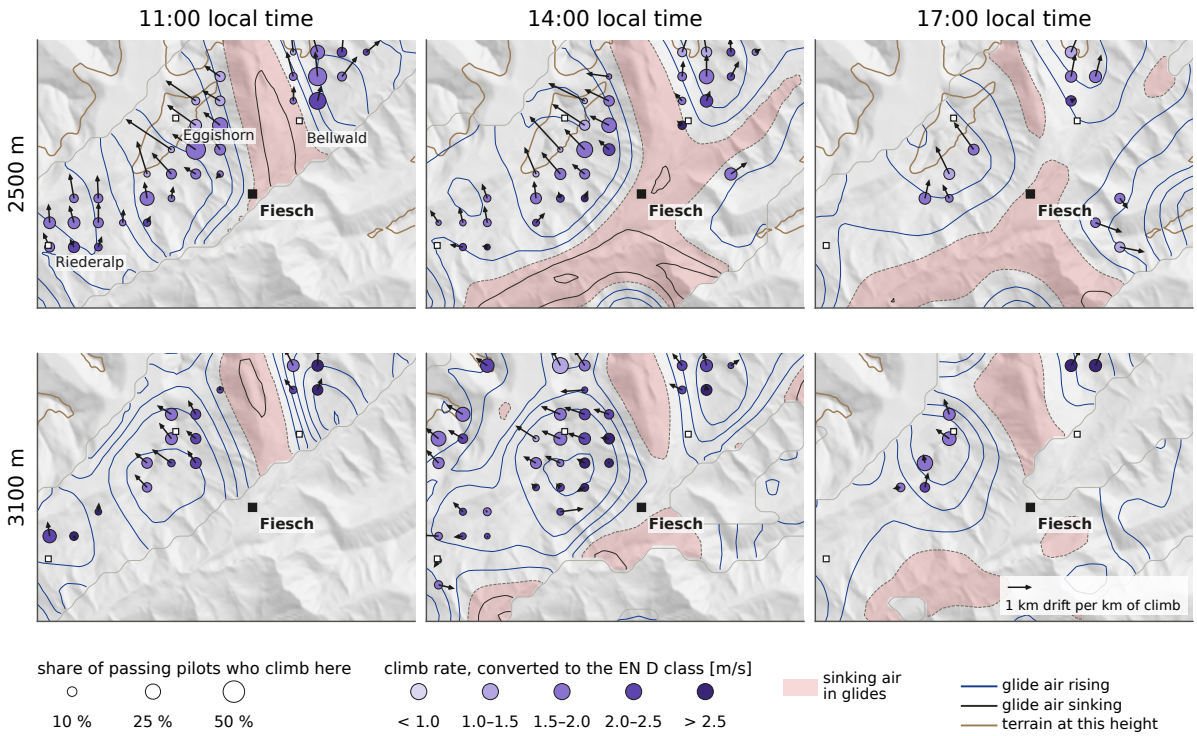

Figure 10: Thermals and flow field above Fiesch, at 2500 m (top) and 3100 m (bottom), at 11:00, 14:00 and 17:00 local time, all days; the area is about 15 by 11 km. Lines: flow field from the glides as in Figure 8, contours every 0.2 m s^{-1}, blue rising, dark grey sinking, shaded where the air sinks. Circles: thermals on a 1 km grid, from the climbs through the 200 m band within ±1 h; area: share of the pilots passing through the cell within the band who climb there; shade: median climb rate, converted to the EN D class with the polars; arrows: mean drift per 1000 m of climb. Only cells with at least 25 passing pilots and five climbs are shown, arrows from ten climbs. Brown: terrain at the height of the map. Squares: Riederalp, Eggishorn, Bellwald and Fiesch.

5.4 A test on years not used

A flow field is useful only if it predicts the air on days that did not contribute to it. We test this by leaving out one year at a time, building the flow field from the remaining years, and predicting the air of every glide segment of the year left out, on days with at least ten flights (1 725 days with usable segments; 1.83 million segments, 34 300 glide hours). For this test the flow field is computed in 0.5 km cells and 400 m height bands. The skill is measured as

$$R^2 = 1 - \frac{\sum_s \Delta t_s \, (w_s - \hat{w}_s)^2}{\sum_s \Delta t_s \, (w_s - \bar{w}_{\text{band}})^2}, \tag{9}$$

where $\hat{w}_s$ is the prediction and $\bar{w}_{\text{band}}$ the mean of the training years in the height band of the segment.

A single climatological map explains $R^2 = 0.137$ of the variance of single segments (Figure 11a), 0.12–0.17 below 3000 m and less higher up, where fewer flights contribute. Maps per time of day, rescaled linearly with the thermal strength of the hour (the median climb rate of the circling pilots in that hour of the same day), raise this to 0.143. For means over a day, a 5 km tile and a 400 m band (84 743 groups with at least 300 s of glides), the climatological map explains 0.304 and the time-of-day map 0.319. To judge these numbers we measure how much of the variance is tied to place and time at all. For each segment we draw a partner segment of another flight in the same 1 km cell, 300 m height band and hour, and correlate the deviations of the two from the mean of their height band, weighted by duration. On the same day the two

segments share 35 % of their variance (46 % for segments of at least 60 s); on days of other years they share 15 % (18 %). The climatological map built from other years, with $R^2 = 0.137$, thus captures nearly all that place and time of day carry from year to year; the partner test works on a slightly coarser grid, so the comparison is approximate. A further fifth of the variance is shared by gliders on the same day: the weather of the day, which a map from other years cannot contain. About two thirds are not shared even by two gliders at the same place and hour of the same day: thermals and turbulence on scales below the cell, and measurement noise. The root-mean-square error of a single segment is $0.88\,\mathrm{m\,s^{-1}}$. The thermal strength of the hour, and in the next version the drift of nearby thermals, are taken from the climbs of the same day: these versions describe the air given what the climbs of that day show, not a forecast.

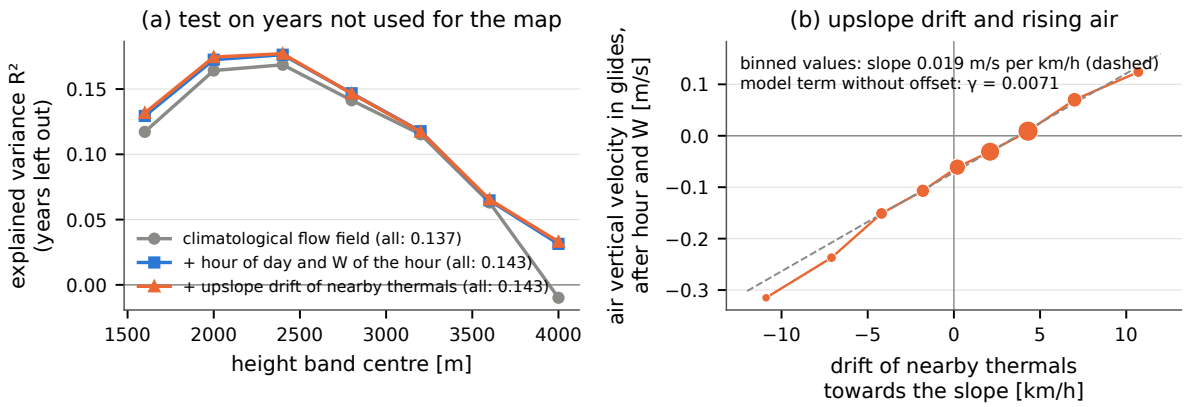

Figure 11: (a) Explained variance of the air vertical velocity of single glide segments in years not used to build the flow field, per height band, for three versions of the flow field: a single climatological map; maps per time of day rescaled with the thermal strength of the hour; and the latter plus a term in the upslope drift of nearby thermals. (b) Air vertical velocity in glides after removing the time-of-day map, against the component of the drift of thermals within about 3 km, 300 m and 1 h on the same day directed up the local slope; marker area grows with glide hours; dashed: weighted linear fit to the binned values.

The drift of thermals near a glide, their horizontal speed from the wind estimate of the circling phases (Section 2), carries information about the local circulation. Figure 11b shows the air vertical velocity in glides, after removing the time-of-day map, against the component of this drift towards the local slope. The relation is close to linear, from $-0.32\,\mathrm{m\,s^{-1}}$ at $-11\,\mathrm{km\,h^{-1}}$ (drift away from the slope) to $+0.12\,\mathrm{m\,s^{-1}}$ at $+11\,\mathrm{km\,h^{-1}}$ (towards it), with a slope of $0.019\,\mathrm{m\,s^{-1}}$ per $1\,\mathrm{km\,h^{-1}}$ (weighted fit to the binned values; offset $-0.071\,\mathrm{m\,s^{-1}}$ at zero drift). In the predictive version of the flow field this term was fitted without an offset, $\gamma = 0.0071\,\mathrm{m\,s^{-1}}$ per $1\,\mathrm{km\,h^{-1}}$ (range 0.0066–0.0076 over the years left out). It leaves R^2 for single segments at 0.143 and raises that of day-and-tile means from 0.319 to 0.322: large drifts are rare, and part of the local circulation is already contained in the map.

The polars themselves were fitted from all years. Refitting the polar of every type without the year left out, and computing the air of that year with these polars, changes the polars by $0.006\,\mathrm{m\,s^{-1}}$ at $40\,\mathrm{km\,h^{-1}}$ in the median (90th percentile $0.022\,\mathrm{m\,s^{-1}}$) and R^2 from 0.1371 to 0.1369 for single segments and from 0.3039 to 0.3035 for day-and-tile means (Appendix A). A common offset of all polars cannot change the test at all, since it shifts training and test segments alike. A common tilt of all polars does, because it correlates the air with the airspeed, which itself varies with place and hour: the tilt of Section 3.7 raised R^2 from 0.130 to 0.137, and a further tilt of $0.01\,\mathrm{m\,s^{-1}}$ per $1\,\mathrm{km\,h^{-1}}$ about $40\,\mathrm{km\,h^{-1}}$, the size of the correction itself and beyond the upper end of its interval, would change the map of Figure 8 by -0.09 to $+0.10\,\mathrm{m\,s^{-1}}$ in 95 % of its cells (correlation 0.997) and raise R^2 to 0.143. The uncertainty of the tilt thus enters the flow field as a pattern of this size, correlated with the airspeeds flown; it does not change where the air rises and where it sinks.

The flow field hardly depends on the glides above the window. Without them, 20 % of the glide time, the maps of Figure 8 change by less than 0.15 m s^{-1} in 95 % of the cells (correlation 0.99), most of it a common shift of +0.07 m s^{-1}, since fast glides lie in sinking air; R^2 changes from 0.137–0.143 to 0.127–0.134. The glides below the window lie in rising air: without them as well, the maps keep their pattern (correlation 0.97) but shift by −0.06 m s^{-1}.

6 What climbs measure

Hernández-Aguayo et al. (2026) and this study use the same kind of data for different questions. Theirs covers a whole country at the scale of a reanalysis cell and one hour and asks which meteorological variables control the thermals; boundary-layer height emerges as the leading predictor of ceiling and climb rate. Ours covers one valley system on a 0.5 km grid and asks how the air moves along the glides. Both read the air from the motion of gliders, and both need to know what else that motion contains.

A climb rate is the vertical velocity of the air on the pilot's circle minus the sink of the glider in the turn. Hernández-Aguayo et al. (2026) take this sink as 1.0–1.2 m s^{-1} for all gliders and the mean climb rate of all pilots as the thermal strength. On average the sink is about right: from the polars and the turn times below, the median sink in the turn is 1.20 m s^{-1}. But a climb rate contains four quantities besides the air, and they differ between gliders, heights and pilots (Figure 12a).

1. *The glider.* At 35 km h^{-1}, the closest of our bands to circling speed, the flight-weighted class means differ by 0.09 m s^{-1} between EN B and EN D, and the only EN A type with a polar sinks 0.33 m s^{-1} faster than the competition glider (Section 4.3).

2. *The height.* In thinner air a glider sinks faster (Section 3.2): the EN D class by 0.05 m s^{-1} more at 2000 m than at 1000 m, and by 0.11 m s^{-1} more at 3000 m.

3. *The bank angle.* The segmented logs give the duration and the number of turns of each circling piece, hence the turn time T. With the airspeed v of minimum sink from the polar, $2\pi/T = g \tan\beta/v$ gives the bank angle β; at constant angle of attack the sink grows by $1/\cos^{3/2}\beta$. The median turn takes 27 s, with a radius of 45 m and a bank of 14°; the turn adds 0.03–0.08 m s^{-1} (quartiles) to the sink. Irregular circles, while a pilot centres, lengthen the turn time, so this is a lower bound.

4. *The pilot.* Pilots centre a thermal with different skill. In climbs shared by at least three pilots we compare, for each pilot and 200 m height band, the time needed to cross the band while circling with that of the other pilots crossing the same band within 300 m and 5 min (108 600 crossings on 966 days). To separate skill from chance, pilots are selected in one band and measured in the next band of the same climb. The upper quarter then climbs 0.35 m s^{-1} (95 %: 0.33–0.36) faster than the others, the best tenth 0.53 m s^{-1} (0.50–0.55). Within 150 m and 1 min, where pilots share the same part of the thermal at the same moment and not different pulses of it, the advantage is 0.15 m s^{-1} (0.12–0.18) and 0.24 m s^{-1} (0.20–0.30). Removing the sink of the gliders with the polars changes none of these values by more than 0.01 m s^{-1}. The advantage is smaller in gaggles of more than ten pilots, presumably because the others mark the core.

Glider, height and bank angle can be removed with the polars, the density and the turn time; a climb then becomes a measurement of the air on the pilot's circle. The pilot can only be bounded. A fifth property cannot be removed: pilots circle only where the air rises faster than their glider sinks in the turn, so the climbs sample the upper tail of the air. Along the glides the air rises

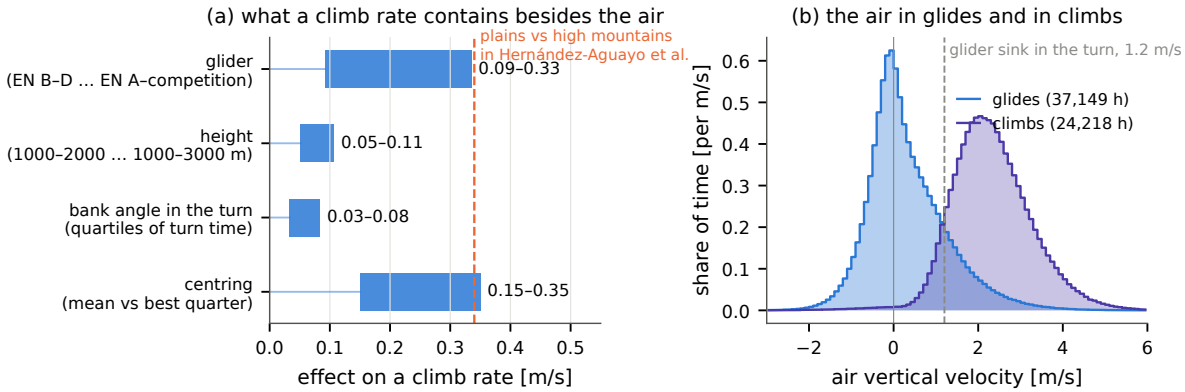

Figure 12: What a climb rate contains besides the air. (a) Size of four effects, each bar from a smaller to a larger comparison: glider (sink at 35 km h^{-1}, flight-weighted class means, EN B against EN D to the EN A type against the competition glider), height (sink of the EN D class at 1000 m against 2000 to 3000 m), bank angle (additional sink in the turn, quartiles of the turn time), pilot (all others against the best quarter in the same thermal, narrow to wide window). Dashed: difference of the mean climb rate between plains and high mountains in Hernández-Aguayo et al. (2026). (b) Air vertical velocity along the glides and in the climbs (climb rate plus the sink of the glider in the turn, from its polar, the density and the turn time), weighted by time, 1400–4200 m, flights with a type polar. Dashed: median sink of the glider in the turn.

faster than 1.20 m s^{-1} during 16 % of the time; in the climbs it rises at 2.3 m s^{-1} on average (Figure 12b).

A constant offset would not change the correlations of Hernández-Aguayo et al. (2026). But gliders, pilots, heights and the selection change with terrain, season and the strength of the day, and the glider and pilot effects are each of the size of the difference they find between plains and high mountains, 1.01 against 1.35 m s^{-1} in the warm season. Part of that difference may belong to gliders and pilots rather than to the air; the height acts the other way, for climbs over high mountains lie higher, where gliders sink more. Our own thermal strength W (Section 2.2) is a climb rate too; it serves only as an index of the day, and only the product cW enters the polars.

The glides add information that the climbs do not contain. They sample the air between the thermals, they show where it rises without circling and where it sinks, and they do so at the resolution of the terrain, with only the polar to remove. Hernández-Aguayo et al. (2026) name the transition phases as a natural extension of their pipeline, for the spacing of thermals; to read the vertical motion of the air along the glides, the polars are needed.

7 Discussion

The assumption about speed. All quantities in this paper are conditional on where and when pilots fly: on flyable days, along chosen lines, mostly in spring and summer, and at speeds chosen according to the air. The polars rest on the assumption that within the window of its class pilots glide through ordinary air. Within the window it is supported by the bands lying on the two-parameter physical curve, by the quiet seconds giving the same mode as all seconds, and by a subsidence slope that is the same at all airspeeds. It holds only approximately, and the part that fails is measured and removed: the choice of speed steepens the mode by 0.12 m s^{-1} per 10 km h^{-1} (0.02–0.27), measured separately for the narrow and the wide windows with the same result, and the polars are tilted back by this amount, in a loop in which the polars used to measure the air of the neighbours are the polars obtained (Section 3.7). What remains is the uncertainty of that number, a factor of two either way at its 95 % limits, which the intervals of the polars carry: at the most flown airspeed of a type nothing changes, at the ends of its window

the interval widens from ± 0.03 to about $\pm 0.06\,\mathrm{m\,s^{-1}}$ for the narrow windows and $\pm 0.12\,\mathrm{m\,s^{-1}}$ for the wide ones and becomes asymmetric. Comparisons between gliders of the same group of windows, the harness experiment and the pattern of the flow field do not depend on it. Within the window the points also lie slightly flatter than the physical curve, higher at its ends than in its middle (Section 3.6); the tilt, being linear, does not change this bending. An error of the airspeed of the single second does not explain it, although such an error moves seconds towards the most flown airspeed: placing every band at the mean airspeed actually flown by its seconds, recovered from the measured distribution of airspeeds and the measured scatter of the single second, $5.1\,\mathrm{km\,h^{-1}}$, makes the points steeper but leaves them as straight as before. More likely, the special air does not begin abruptly at the edge of the window but grows gradually towards both ends; in addition, below trim speed pilots brake, which changes the shape of the wing. The logs do not separate the two. The effect is about half the 95 % interval of a single type, but for the EN A, B and C classes it means that the shape of the polar, within the window and beyond, rests on the physical form and not on the points. With the tilt of Section 3.7, the extension of these narrow windows places the best glide ratio of the EN A, B and C types at 44–49 $\mathrm{km\,h^{-1}}$ (median per class), beyond their windows; this optimum is a property of the extended curve, not of the points, and Table 3 therefore gives for these types the glide ratio at the end of the window, marked as a bound; the optimum of the extension itself is not given, since the tilt enters it with the full lever of the extension and single types would reach glide ratios of 12 and more at 50–57 $\mathrm{km\,h^{-1}}$, which no points support. In the classes with wide windows this form carries $5\,\mathrm{km\,h^{-1}}$ beyond a narrow window to within 0.01–0.03 $\mathrm{m\,s^{-1}}$ (Appendix C), which is the error to expect for the EN A, B and C polars up to about $45\,\mathrm{km\,h^{-1}}$. Outside the window the results do not depend on the assumption: the polars use no glide there, and the flow field hardly changes without the glides above it.

What a polar of a type means. A type polar averages over sizes, wing loadings, trims and harnesses as flown in the Valais. Wing loading moves a polar along a line through the origin by the square root of the load factor; we do not know the loads. The harness, as the Enzo 3 shows, changes the drag term measurably. A polar in this paper is therefore the polar of a type as it is flown, not of a type as certified. With a few hundred flights, a type obtains a polar with an interval of a few hundredths of a metre per second at its most flown airspeed. This is enough to follow a model line through its generations (Appendix D lists the types of each model line by year of release): the sink of the Sigma at its most flown airspeed, 35–38 $\mathrm{km\,h^{-1}}$, decreases from $1.19\,\mathrm{m\,s^{-1}}$ for the Sigma 7 (2008) to 1.17 for the Sigma 8 and $1.11\,\mathrm{m\,s^{-1}}$ for the Sigma 10 (2017), and the Sigma 11 and Sigma DLS, flown faster, sink 1.15–1.16 $\mathrm{m\,s^{-1}}$ at their own most flown airspeed; part of such differences may reflect the age of the wings and the harnesses flown with them. Polars of this kind complement test flights and wind-tunnel measurements. They are polars of a fleet of pilots, and only where the fleet is broad enough: a type whose logs come mostly from one pilot gets no polar (Section 3.6), because what one pilot flies, with one harness and one weight, is not a property of the type. The faired race harness is the clearest example: it belongs to the pilot, and it enters the polar of a type exactly in the share of its flights flown with one, which the Enzo 3 shows for a whole class of pilots and one excluded EN D type shows for a single pilot.

Which flights. Only flights with a recognisable glider name contribute to the polars, and only flights of types with a polar contribute to the flow field: 25 546 of 86 190 flights, 24 949 of them with usable glides, biased towards recent gliders. Outside its window a polar is an extension of the physical form, not a measurement; a few kilometres per hour beyond the window the extension is good to a few hundredths of a metre per second, farther out it is not tested. For the EN A, B and C types the window ends between 35 and 43 $\mathrm{km\,h^{-1}}$, so their polars with the speed bar pushed need an independent measurement, such as flights with a calibrated airspeed sensor

in still air. The absolute level rests on the still-air limit and on 63 flights without thermals.

A second quantity from the same logs. A flight recorder writes two altitudes per second: a barometric altitude, which is the measured pressure expressed in the standard atmosphere, and a GNSS altitude. Between two pressure levels the hypsometric equation turns the GNSS thickness into the mean virtual temperature of the layer, with no temperature sensor involved. Along each flight, within each 25-hPa layer, a regression of the GNSS altitude on the logarithm of the pressure gives the temperature of the layer, and the median over the flights of a day gives a daily profile over the flown slopes. Against the Payerne radiosonde, 100 km away on the Swiss Plateau, the 10–14 UTC profiles of 375 days (2011–2026, dedicated flight instruments only) agree in the layer 2000–3600 m to a median of +0.6 K with a day-to-day spread of 1.5 K; below 2200 m the valley atmosphere is 2–4 K warmer than the Plateau, as it should be (Figure 13). Instruments that silently recalibrate their barometer, smartphones and logs before 2011 have to be excluded. The same logs thus give both the vertical motion of the air and the temperature of the column it moves in; what this profile shows about the heating of the valley atmosphere and the ceiling of the thermals is beyond the scope of this paper.

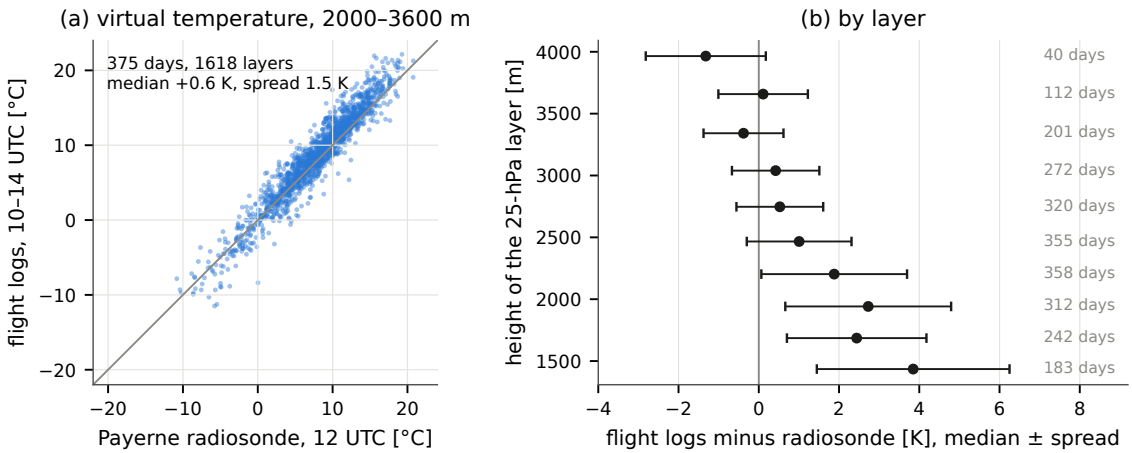

Figure 13: Layer temperature from the barometric and GNSS altitudes of the flight logs, checked against the Payerne radiosonde (12 UTC), 2011–2026, flights with dedicated instruments. (a) Virtual temperature of the 25-hPa layers between 2000 and 3600 m, median over the flights of each day between 10 and 14 UTC, against the radiosonde; grey: identity. (b) Flight logs minus radiosonde by layer: median and spread (median absolute deviation, scaled) for layers with at least 20 days.

Beyond one valley. The method needs nothing but enough logs per glider type. In other regions some assumptions will be tested harder than in the Valais. Where glides go mostly in one direction, a wind error no longer cancels between headwind and tailwind, and the polar should be computed separately for both, which must agree if the wind is right. Where thermals are much stronger, the proportionality of equation (5) must be checked before it is extrapolated, and the thermal strength of a day has to be defined for a region rather than a valley. Glider names in other languages will need more care.

8 Conclusions

Paraglider flight logs become measurements of the air once the sink polar of the glider is known, and the polars can be measured from the logs themselves. At the airspeeds flown most, glider and pilot are a constant and the air is not, so the most frequent vertical speed in straight flight

there is the sink of the glider. Pilots keep other speeds for special air: slow flight for lift, fast flight for strong sink and for the rising air in which they leave a thermal. The physical form of the polar shows for each class where glider and pilot are constant: in a window around the most flown airspeed, 32–40 km h^{-1} for EN B and C and 34–48 km h^{-1} for EN D, the points follow the physical curve; outside it they show the special air, and only the window is used. Within the window the constancy is approximate: the air that other pilots find at the same place and time, measured with neighbourhoods from 2 km down to 250 m, shows that the choice of speed steepens the most frequent value by 0.12 m s^{-1} per 10 km h^{-1} (0.02–0.27), for gliders with narrow and with wide windows alike; the polars are corrected for it in a loop until the polars used for the neighbours are the polars obtained, and the uncertainty of the correction is carried into their intervals. Corrected for air density, for the subsidence of the glide air and for the choice of speed, and fitted with the physical form in 1 km h^{-1} bands, the most frequent value gives polars with typical 95 % intervals of $\pm$0.02–0.03 m s^{-1} at the most flown airspeed for 73 types, wider towards the ends of the window; types whose polar depends on one pilot are excluded; a common offset of all polars of up to about 0.1 m s^{-1} cannot be excluded. Fast glides are rare, and the flow field does not need them: without the glides above the window it changes by less than 0.1 m s^{-1} in 95 % of its cells. The subsidence correction is measured from the flights themselves; it grows linearly with the thermal strength of the day, by 0.12 m s^{-1} per 1 m s^{-1}, and is the same at all airspeeds within its uncertainty. In a natural experiment, the method detects a change in the polar of one glider that coincides with the arrival of a faired race harness and grows with speed, as a lower drag requires; in a second, one wing in two cloths, measured from two independent sets of flights, gives the same polar to 0.01 m s^{-1}.

With the polars removed, glide segments become measurements of the air. Over the Valais they show rising air over sunlit slopes and ridges, compensating subsidence over the valley centre in the afternoon, and a dependence on the local drift of thermals. A flow field built from other years, with polars built without those years, explains a modest but robust part of the variance of single glides and about a third of the variance of daily means over 5 km tiles; the rest is the weather of the day and variability below the scale of the maps. Above Fiesch, the climbs add the thermals: where they stand, how often they are found, how strong they are and how they lean. Glider polars are thus the step that turns the glides in flight logs into observations of the air. Climbs, too, become measurements of the air once glider, height and bank angle are removed with the polars, the density and the turn time; the centring of the pilot and the choice of where to circle remain, and the pilot effect alone is of the size of the differences that climb-based studies compare.

The flow field is a climatological mean for one valley system. It can serve as a coarse guide for pilots and as the environment for simulations of cross-country flight, in which synthetic pilots fly a measured polar through the measured air. Extended to the Alpine arc, with the gaps between flown paths filled, such simulations may identify routes that have not yet been flown and quantify what a difference between two polars is worth on a given route. The flow field may also serve as an observational reference for models of slope and valley circulations. The same logs carry a second quantity: from their barometric and GNSS altitudes the temperature of every 25-hPa layer follows, within 1.5 K of the Payerne radiosonde, so the platform measures the motion of the air and the state of the column it moves in.

Data and code availability

The flight logs were provided by XContest for this study; they are not public. Pilot names appear in the log headers; they were replaced by an anonymous key to count the pilots per type (Section 3.6) and are neither stored nor published. The segmentation and histogram code (`flightstates` 2.2, `polarmaker` 1.4) is openly available (Korner, 2026). The polars

of Appendix D are available in machine-readable form at https://joerxc.org/Korner_2026_polars.csv. The scripts that compute the polars, the flow field and the figures of this paper are available from the author.

Acknowledgements

We thank XContest for providing the flight logs and the pilots who recorded and uploaded them.

Declarations

Funding. The author received no funding for this work.

Competing interests. The author declares no competing interests. The author is a paraglider pilot and flies gliders of some of the types in Appendix D.

Author contribution. J. Korner designed the study, wrote the code, analysed the data and wrote the paper.

References

Zsuzsa Ákos, Máté Nagy, and Tamás Vicsek. Comparing bird and human soaring strategies. *Proceedings of the National Academy of Sciences*, 105(11):4139–4143, 2008. doi: 10.1073/pnas.0707711105.

John D. Anderson, Jr. *Introduction to Flight*. McGraw-Hill Education, New York, 8th edition, 2016. ISBN 978-0-07-802767-3.

H. Babinsky. The aerodynamic performance of paragliders. *The Aeronautical Journal*, 103(1027): 421–428, 1999. doi: 10.1017/S0001924000027974.

Louis Berthus. Aerodynamic performances of a fairing in paragliding. Master's thesis, Université de Liège, 2024. URL https://matheo.uliege.be/handle/2268.2/20861. Accessed 2026-10-06.

J. R. Cook and L. A. Stefanski. Simulation–extrapolation estimation in parametric measurement error models. *Journal of the American Statistical Association*, 89(428):1314–1328, 1994. doi: 10.1080/01621459.1994.10476871.

F. Couvreux, F. Hourdin, and C. Rio. Resolved versus parametrized boundary-layer plumes. Part I: A parametrization-oriented conditional sampling in large-eddy simulations. *Boundary-Layer Meteorology*, 134(3):441–458, 2010. doi: 10.1007/s10546-009-9456-5.

Cross Country. Ozone release Zeolite GT. Cross Country Magazine, 18 February 2020, 2020. URL https://xcmag.com/news/ozone-release-zeolite-gt/. Accessed 2026-10-14.

Cross Country. Ozone Submarine harness review. Cross Country Magazine, 8 January 2024, 2024. URL https://xcmag.com/?p=86005. Accessed 2026-10-06.

Tom G. Farr, Paul A. Rosen, Edward Caro, Robert Crippen, Riley Duren, Scott Hensley, Michael Kobrick, Mimi Paller, Ernesto Rodriguez, Ladislav Roth, David Seal, Scott Shaffer, Joanne Shimada, Jeffrey Umland, Marian Werner, Michael Oskin, Douglas Burbank, and Douglas Alsdorf. The Shuttle Radar Topography Mission. *Reviews of Geophysics*, 45(2):RG2004, 2007. doi: 10.1029/2005RG000183.

Peter F. Heatwole. Parametric paraglider modeling. Master's thesis, California Polytechnic State University, San Luis Obispo, 2022. Software: `https://github.com/pfheatwole/glidersim`.

César Hernández-Aguayo, Matthieu Cristelli, and Michael Benzaquen. From flight logs to atmospheric science: Paragliders as convection sensors for identifying thermal predictors, 2026.

Manual of the ICAO Standard Atmosphere: Extended to 80 Kilometres (262 500 Feet). International Civil Aviation Organization, 3rd edition, 1993. ICAO Doc 7488/3.

Jörg Korner. fine-segmenter: flightstates 2.2 and polarmaker 1.4. GitHub repository, 2026. URL `https://github.com/joergkorner/fine-segmenter`. Commit 1da4b8f, 6 October 2026.

Robert Kulhánek. Identification of a degradation of aerodynamic characteristics of a paraglider due to its flexibility from flight test. *Aircraft Engineering and Aerospace Technology*, 91(6):873–879, 2019. doi: 10.1108/AEAT-06-2018-0162.

Paul B. MacCready, Jr. Optimum airspeed selector. *Soaring*, page 10, January–February 1958.

D. Marsden. Sailplane performance flight testing. *Technical Soaring*, 9(1):23–32, 1985.

E. A. Nadaraya. On estimating regression. *Theory of Probability & Its Applications*, 9(1):141–142, 1964. doi: 10.1137/1109020.

Ozone Paragliders. New from Ozone – THE SUBMARINE. Ozone news, 2021. URL `https://flyozone.com/paragliders/news/new-from-ozone-the-submarine`. Accessed 2026-10-06.

Harlan D. Shannon, George S. Young, Michael A. Yates, Mark R. Fuller, and William S. Seegar. Measurements of thermal updraft intensity over complex terrain using American white pelicans and a simple boundary-layer forecast model. *Boundary-Layer Meteorology*, 104(2): 167–199, 2002. doi: 10.1023/A:1016095804357.

W. F. Teskey, D. H. Adler, and W. J. Teskey. Determining free flight performance by surveying engineering techniques. *Journal of Surveying Engineering*, 132(2):93–96, 2006. doi: 10.1061/(ASCE)0733-9453(2006)132:2(93).

Jelle Treep, Gil Bohrer, Judy Shamoun-Baranes, Olivier Duriez, Renato Prata de Moraes Frasson, and Willem Bouten. Using high-resolution GPS tracking data of bird flight for meteorological observations. *Bulletin of the American Meteorological Society*, 97(6):951–961, 2016. doi: 10.1175/BAMS-D-14-00234.1.

Jérémie Vilpellet, Alexandre Darmon, and Michael Benzaquen. From random walks to thermal rides: Universal anomalous transport in soaring flights, 2026.

Jörg Wagner. On the identification of the speed polar during normal soaring flight. *Technical Soaring*, 18(2):49–54, 1994.

Bastienne Wentzel. The harness files: Part 3. Cross Country Magazine, 6 September 2024, 2024. URL https://xcmag.com/gear-guide/design-insights/the-harness-files-part-3. Accessed 2026-10-06.

XContest. XContest, 2026. URL https://www.xcontest.org. Accessed 2026-10-06.

Dino Zardi and C. David Whiteman. Diurnal mountain wind systems. In Fotini K. Chow, Stephan F. J. De Wekker, and Bradley J. Snyder, editors, *Mountain Weather Research and Forecasting: Recent Progress and Current Challenges*, Springer Atmospheric Sciences, pages 35–119. Springer, Dordrecht, 2013. doi: 10.1007/978-94-007-4098-3_2.

A Tests of the method

Above the window the gliders appear to sink less than the curve predicts (Section 4.2). We tested the obvious causes of this deviation on the 5 309 flights of the EN D types on days with known W, read directly from the logs with the glider name of the log header (a selection slightly different from Table 1), with the airspeed in 1 km h^{-1} bands from 35 to 60 km h^{-1} and a curve fitted to 35–45 km h^{-1} for every variant, a common range inside the window of the class, 34–48 km h^{-1}, so that the variants can be compared (Figure 14). (i) Errors of the airspeed move seconds from the populated slower bands into the sparse fast ones. The vario is averaged over about 30 s, whereas the airspeed is that of the single second, which scatters by 5.1 km h^{-1} around its 30-s average. Removing this error, by binning the seconds by the airspeed averaged like the vario, or by adding further error of 2, 4 and 6 km h^{-1} and extrapolating back to none (Cook and Stefanski, 1994), shifts all bands but leaves the deviation above 47 km h^{-1} as it is. (ii) The exchange of speed and height when the pilot accelerates or slows down: a total-energy vario, which adds $v\,\dot{v}/g$, shows the same deviation. (iii) Errors of the wind estimate: the deviation grows with the wind, but it is present when the wind is below 7 km h^{-1}. (iv) Selection of flights: it is present in the quarter of flights with the most seconds above 50 km h^{-1} as in the other flights, and on weak as on strong days. Three further restrictions leave the deviation unchanged within its uncertainty: to seconds with a steady airspeed over the averaging window of the vario and no circling within 30 s, to seconds within two minutes of a thermal, where the wind is measured, and to a vario computed from the GNSS altitude instead of the pressure altitude.

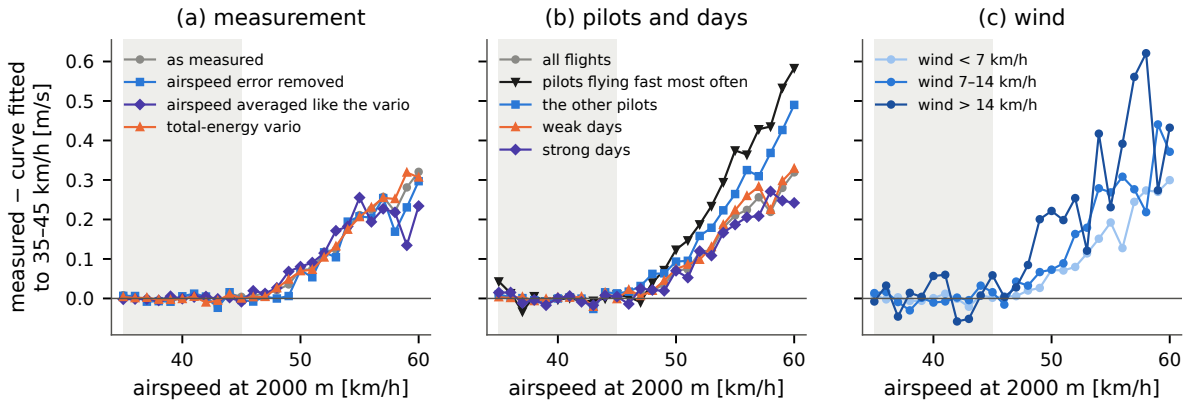

Figure 14: Deviation of the most frequent value from the curve fitted to 35–45 km h^{-1} (shaded), EN D class (5 309 flights read from the logs), 1 km h^{-1} bands at 2000 m, after the subsidence correction; positive for less sink. Each variant has its own curve. (a) As measured; with the error of the airspeed removed by extrapolation from added errors of 2, 4 and 6 km h^{-1}; with the seconds binned by the airspeed averaged like the vario; with a total-energy vario. (b) The quarter of flights with the largest share of seconds above 50 km h^{-1} and the other flights; days with W below and above 0.9 m s^{-1}. (c) Seconds with an estimated wind below 7, between 7 and 14, and above 14 km h^{-1}.

Two choices of the method were tested on all 6 098 flights of the EN D types read directly from the logs, on all days, since no subsidence correction is needed for this test (Table 2). Narrowing the airspeed band from 5 to 1 km h^{-1} changes the mode by at most 0.01 m s^{-1}; the interval of a single band widens because seconds are lost, but many narrow bands constrain the curve better than a few wide ones. Recomputing the airspeed with half and with one and a half times the measured wind changes the mode by at most 0.02 m s^{-1} between 35 and 45 km h^{-1} and by 0.03 m s^{-1} at 50 km h^{-1}. Glides in the Valais are flown in all directions, so an error of the wind acts in opposite directions on headwind and tailwind seconds and largely cancels.

Table 2: Sensitivity of the mode (m/s, EN D class, 6 098 flights, at 2000 m, before the subsidence correction) to the width of the airspeed band and to a scaling of the wind used to compute the airspeed. In brackets: 95 % interval from resampling flights.

	35 km h^{-1}	40 km h^{-1}	45 km h^{-1}	50 km h^{-1}
band 1 km h^{-1} (fit)	−1.096	−1.173	−1.308	−1.438
band 2 km h^{-1}	−1.095	−1.174	−1.304	−1.445
band 3 km h^{-1}	−1.098	−1.173	−1.301	−1.452
band 5 km h^{-1} (tables)	−1.097	−1.174	−1.304	−1.447
	(−1.105, −1.089)	(−1.182, −1.167)	(−1.313, −1.294)	(−1.459, −1.431)
band 7 km h^{-1}	−1.101	−1.176	−1.299	−1.439
wind ×0.5	−1.080	−1.163	−1.296	−1.448
wind ×1.5	−1.115	−1.186	−1.298	−1.417

Polars by year and without a year. Polars of single years scatter around the polar of all years: for the EN D class the measured sink at 45 km h^{-1} lies between −1.07 and −1.19 m s^{-1} for the years 2018–2026 (all years: −1.14; intervals of single years ±0.07 to ±0.09, most of it the common uncertainty of the tilt), for the Enzo 3 between −1.00 and −1.15 m s^{-1}, with 2024 and 2026 the lowest (Section 4.4). Leaving one year out of the polar of a type changes its sink at 40 km h^{-1} by 0.006 m s^{-1} in the median over 726 type-year combinations, by 0.022 m s^{-1} at the 90th percentile and by 0.12 m s^{-1} at most, for a type with few years. These polars without a year are used in Section 5.4.

B Measuring the tilt

Pilots choose their speed according to the air also within the window (Section 4.2). To measure how much of this reaches the most frequent value, the air at the place and time of each glide segment is measured with other pilots: the duration-weighted mean of the air vertical velocity, from equation (7), of all glide segments of other flights on the same day in the same cell, height band and time span, flown at 35–43 km h^{-1}, where the polars of all types are most precise. For the glides of a class with such neighbours, the most frequent vertical speed per 1 km h^{-1} band is then formed twice from the same glide segments, weighted by duration: once with the day correction $c\,W$ as in the paper, and once with the neighbours' air subtracted instead. The physical curve is fitted to both in the window of the class, and the difference of the slopes of the two curves is the part of the air that the choice of speed carries into the polar. The level of the neighbour-corrected curve is not independent of the polars, since the neighbours' air is computed with them, so only the slope is compared. Because this test works on glide segments and only on those with neighbours, its curves are not the polars of Appendix D; only their difference is used.

Neighbours see only part of the air at the glide, and the closer they are, the more of it. The measurement is therefore made with four neighbourhoods: cells of $s = 2$, 1, 0.5 and 0.25 km, height bands of 300s m and time spans of 10s min (the same or an adjacent span, so up to 20s min apart). Figure 4a shows the band means of the neighbours' air for the EN D class; a straight line through them has a gradient of 0.09, 0.18, 0.26 and 0.30 m s^{-1} per 10 km h^{-1} of the glide's airspeed as the neighbourhood shrinks from 2 km to 250 m, for EN B 0.14, 0.26, 0.36 and 0.38, for EN C 0.13, 0.25, 0.36 and 0.48, for the competition class 0.10, 0.15, 0.17 and 0.23; the weighted mean over the four classes rises from 0.11 to 0.31 and extends to 0.32 at zero size. The change of the slope of the mode when this air is removed is measured per class in the window of the class and combined per group of windows, narrow (measured on EN B and C and applied to EN A as well) and wide (EN D and the competition class), with the inverse variances from resampling

as weights; a weighted straight line through the four sizes gives the value at zero size, from the same resamplings at all sizes so that the line is fitted in every repetition.

Why the first measurement is too small, and the loop. The neighbours' air is computed with the polars of their types, and in the first measurement these are the provisional polars, which carry the tilt being measured. A common offset of all polars is harmless: it shifts the neighbours' air by the same amount at every glide, slow or fast, and cancels in the slope. The tilt is not. Where the air sinks, the neighbours fly a little faster too, and with provisional polars, which are too steep, their air is computed too good there; where the air rises, too bad. This distorts the distribution of the corrected values unevenly between slow and fast glides, and the mode, which is sensitive to the shape of the distribution near its peak, responds to it: with provisional polars the measured tilt is too small. The loop removes the dependence. The tilt is measured with untilted polars, the polars are tilted by the result, the neighbours' air is computed again with the tilted polars and the tilt is measured again. In practice, tilting all polars of a group by δ changes the air of each neighbour by $-\delta\,(v_n - v_h)/f$, with v_n its airspeed, v_h the most flown airspeed of its type and f the density factor to its altitude, so the rounds after the first were computed by applying this change to the neighbours' air directly, which is equivalent to recomputing the polars; undoing the first correction in this way reproduces the first measurement to 0.01 m s^{-1} per 10 km h^{-1} (0.073 against 0.063). The second round, with polars actually corrected by 0.063, was computed directly. For all classes together the sequence is 0.063 (untilted polars; 95 %: 0.009–0.180), 0.123 (polars tilted by 0.063), 0.115 (tilted by 0.123) and 0.150 (tilted by 0.183) m s^{-1} per 10 km h^{-1}: the measurement responds to the tilt of the neighbours' polars with about half of it, so the loop converges, and it converges where the measured tilt equals the assumed one, at about 0.12 (Figure 4c). Per group, with the polars of each group tilted by its own value, two rounds near the fixed point give 0.120 and 0.126 for the narrow windows (assumed 0.123 and 0.120) and 0.099 and 0.131 for the wide ones (assumed 0.118 and 0.100); their means, 0.123 (95 %: 0.021–0.273) and 0.115 (0.020–0.257) m s^{-1} per 10 km h^{-1}, are the tilts of Section 3.7. The per-size values at the end of the loop are +0.05, +0.14, +0.03 and 0.00 m s^{-1} per 10 km h^{-1} for the narrow windows and +0.04, +0.06, +0.14 and +0.10 for the wide ones at 2 km, 1 km, 500 m and 250 m (Figure 4b). Within their intervals the two groups do not differ; each is nevertheless corrected by its own measurement. The share of the neighbours' air that reaches the mode is about a third at zero size: what the mode absorbs is the large-scale part of the air that pilots follow, and the small-scale part, which the close neighbours share, lies in the tails of the distribution and not at its peak. The loop was run with the polars of all 101 types that pass the first two conditions of Section 3.6, before the 28 types whose polar rests on one pilot were excluded. The excluded types enter the measurement only through their flights as neighbours; with the final 73 polars the gradients of the neighbours' air over the window change by less than 0.02 m s^{-1} per 10 km h^{-1} at every size, so the loop was not repeated.

C The extension beyond the window

For the EN A, B and C classes the window spans 8–9 km h^{-1}, and the shape of their polars beyond it rests on the physical form (Section 3.6). The classes with wide windows show how far the form carries. The curve of the EN D class is fitted to a window as narrow as that of EN B, the most flown airspeed ±4 km h^{-1} (35–43 km h^{-1}), and extended; the measured bands up to the edge of the real window, 44–48 km h^{-1}, lie above the extension by +0.013, +0.011, +0.018, +0.019 and +0.026 m s^{-1} at 1 to 5 km h^{-1} beyond it, always in the direction of less sink, as the flattening of the points towards the edges of the window (Section 3.6) implies (Figure 15a). For the competition class, fitted to 37–45 km h^{-1}, the bands 46–51 km h^{-1} deviate by −0.03 to +0.04 m s^{-1} (Figure 15b). Over the 18 EN D and competition types with their own windows, the

median deviation is -0.01 to $+0.01\,\mathrm{m\,s^{-1}}$ at 1 to $5\,\mathrm{km\,h^{-1}}$ beyond the narrow window and the scatter between types 0.03–0.06 $\mathrm{m\,s^{-1}}$. The best glide ratio of the EN D class from the narrow window is 10.84 against 10.99 from the full window, and 11.60 against 11.61 for the competition class (the intervals of these absolute values, about -0.6 to $+1.7$, are dominated by the tilt, which is common to both fits). The extension of a narrow window is thus good to a few hundredths of a metre per second over the next $5\,\mathrm{km\,h^{-1}}$, which covers the EN A, B and C polars up to about $45\,\mathrm{km\,h^{-1}}$; farther out it is not tested.

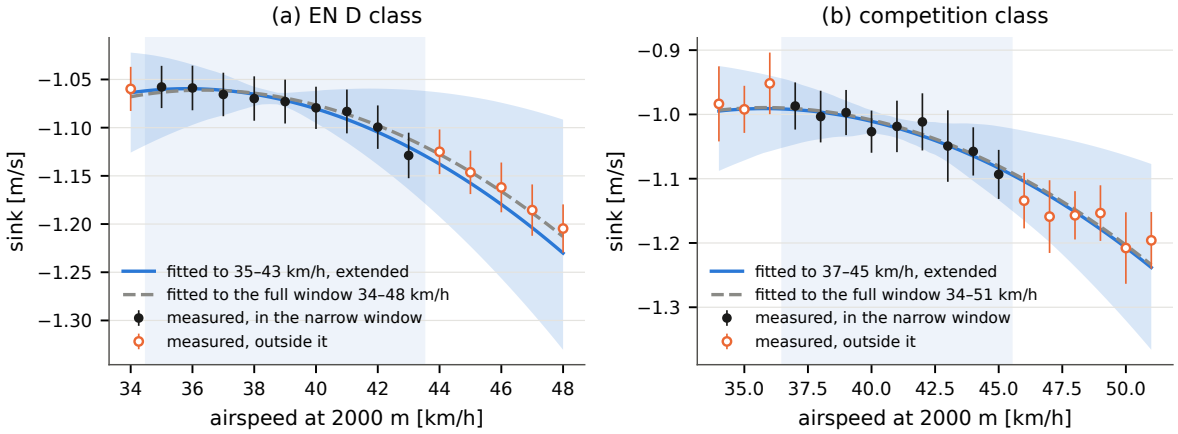

Figure 15: The physical curve fitted to a narrow window, the most flown airspeed $\pm 4\,\mathrm{km\,h^{-1}}$ (shaded), and extended to the edge of the real window of the class, with its 95 % band from resampling flights; dashed: the curve fitted to the full window. Points: most frequent value per $1\,\mathrm{km\,h^{-1}}$ band with 95 % intervals, filled inside the narrow window, open outside. (a) EN D class, 5 096 flights; (b) competition class, 590 flights.

D Polars of all glider types

Table 3: Sink polars of the 73 glider types with at least 100 flights on days with a known thermal strength whose points follow the physical curve within their window, in still air at 2000 m (ISA density), with the subsidence correction $c = 0.118$ (Section 3.5) and the correction for the choice of speed, a tilt about the most flown airspeed of $0.123\,\mathrm{m\,s^{-1}}$ per $10\,\mathrm{km\,h^{-1}}$ for EN A, B and C and $0.115\,\mathrm{m\,s^{-1}}$ per $10\,\mathrm{km\,h^{-1}}$ for EN D and the competition class (Section 3.7). Window: airspeed range of the fit (Section 3.6), the window of the class shifted by the difference between the most flown airspeed of the type and that of its class. s is read from the curve $s = av^3 + b/v$ at three airspeeds inside the window: its start, the most flown airspeed of the type, and its end, each given after the @ in km/h; super- and subscripts give the 95 % interval from resampling flights, which includes the uncertainty of the tilt. †: uncertain polar (at the most flown airspeed, an interval wider than $0.2\,\mathrm{m\,s^{-1}}$ or one side of the interval more than four times the other). $(L/D)_{\max}$ and the minimum sink $s_{\min}$ are properties of the fitted curve, with their 95 % intervals, when their airspeed lies inside the window; when the optimum lies outside, the value at the window edge is given, with the airspeed written as <start or >end: a bound from the points, since the extension beyond the window is not tested there. The intervals of $(L/D)_{\max}$ are wide towards higher values because the uncertainty of the tilt enters at the fast end of the window. MS: 99th percentile of the measured airspeed in glides (km/h, at 2000 m). Year: first certification test or, where none was found, the manufacturer's launch; types are sorted by class, within a class by model line, and within a model line by year, so that each line shows its development steps. Class: EN certification class according to the manufacturers and test reports, for older wings the LTF class (1-2 as B, 2 as C, 2-3 as D); for wings certified in different classes by size or weight, the class of the main sizes at the recommended weight; CCC: competition class. Names are the type names as written by pilots, merged by the rules of Section 2.3. Figures 16 and 17 show the polars with the measured points. Types without polar: too few seconds in the window, points that do not follow the physical curve, or a polar that belongs to a single pilot (Section 3.6): the pilot with the most flights has 30 % of them or more, or without him the polar changes by more than $0.03\,\mathrm{m\,s^{-1}}$ at the most flown airspeed or $0.05\,\mathrm{m\,s^{-1}}$ at the window end.

Type	Year	Class	Flights	Days	Window km/h	a $10^{-4}\,\mathrm{s^2\,m^{-2}}$	b $\mathrm{m^2\,s^{-2}}$	s at window start m/s @ km/h	s at most flown v m/s @ km/h	s at window end m/s @ km/h	$(L/D)_{\max}$ @ km/h	$s_{\min}$ m/s @ km/h	MS km/h
Competition class (1 type)													
Enzo 3	2017	CCC	590	263	34–51	−2.499	−7.40	$-0.99^{+0.06}_{-0.09}$ @ 34	$-1.01^{+0.01}_{-0.02}$ @ 41	$-1.23^{+0.14}_{-0.10}$ @ 51	$11.6^{+1.5}_{-0.4}$ @ 47	$-0.99^{+0.06}_{-0.04}$ @ 36	61
EN D (12 types)													
Mantra 7	2019	D	255	164	34–48	−2.070	−9.03	$-1.13^{+0.04}_{-0.05}$ @ 34	$-1.10^{+0.02}_{-0.02}$ @ 38	$-1.17^{+0.14}_{-0.10}$ @ 48	$11.4^{+1.6}_{-0.9}$ @ >48	$-1.10^{+0.07}_{-0.01}$ @ 40	53
Omega 7	2006	D	130	89	32–46	−2.864	−8.97	$-1.21^{+0.06}_{-0.07}$ @ 32	$-1.18^{+0.03}_{-0.03}$ @ 36	$-1.30^{+0.16}_{-0.10}$ @ 46	$9.8^{+1.4}_{-0.7}$ @ >46	$-1.18^{+0.05}_{-0.03}$ @ 36	52
Omega X-Alps	2015	D	127	76	33–47	−2.731	−7.95	$-1.08^{+0.06}_{-0.06}$ @ 33	$-1.07^{+0.04}_{-0.02}$ @ 37	$-1.22^{+0.15}_{-0.10}$ @ 47	$10.7^{+2.1}_{-0.7}$ @ 47	$-1.07^{+0.05}_{-0.02}$ @ 36	56
Omega X-Alps 3	2019	D	250	165	33–47	−3.007	−7.78	$-1.08^{+0.05}_{-0.06}$ @ 33	$-1.09^{+0.02}_{-0.02}$ @ 38	$-1.26^{+0.14}_{-0.09}$ @ 47	$10.3^{+1.6}_{-0.4}$ @ 46	$-1.08^{+0.04}_{-0.02}$ @ 35	56
Omega ULS	2023	D	258	151	34–48	−2.568	−8.39	$-1.10^{+0.05}_{-0.06}$ @ 34	$-1.10^{+0.02}_{-0.02}$ @ 38	$-1.24^{+0.14}_{-0.10}$ @ 48	$10.8^{+1.4}_{-0.8}$ @ >48	$-1.09^{+0.05}_{-0.02}$ @ 37	54
Peak 6	2022	D	180	133	34–48	−2.723	−7.32	$-1.00^{+0.05}_{-0.07}$ @ 34	$-1.02^{+0.02}_{-0.03}$ @ 38	$-1.20^{+0.15}_{-0.11}$ @ 48	$11.2^{+2.1}_{-0.6}$ @ 46	$-1.00^{+0.05}_{-0.04}$ @ 35	58
XC Racer	2018	D	112	78	36–50	−2.604	−8.26	$-1.09^{+0.07}_{-0.08}$ @ 36	$-1.11^{+0.04}_{-0.04}$ @ 41	$-1.29^{+0.14}_{-0.10}$ @ 50	$10.8^{+1.5}_{-0.4}$ @ 48	$-1.09^{+0.08}_{-0.05}$ @ 36	59
Zeno	2016	D	453	208	34–48	−2.369	−7.86	$-1.03^{+0.04}_{-0.06}$ @ 34	$-1.03^{+0.02}_{-0.01}$ @ 39	$-1.15^{+0.13}_{-0.09}$ @ 48	$11.6^{+1.5}_{-0.8}$ @ >48	$-1.02^{+0.04}_{-0.02}$ @ 37	57
Zeno 2	2022	D	696	225	37–51	−2.664	−7.71	$-1.04^{+0.04}_{-0.05}$ @ 37	$-1.07^{+0.01}_{-0.01}$ @ 41	$-1.30^{+0.14}_{-0.10}$ @ 51	$11.0^{+1.3}_{-0.3}$ @ 47	$-1.04^{+0.04}_{-0.05}$ @ <37	60
Zeolite	2019	D	234	169	34–48	−2.745	−8.09	$-1.09^{+0.06}_{-0.08}$ @ 34	$-1.09^{+0.03}_{-0.03}$ @ 39	$-1.26^{+0.14}_{-0.09}$ @ 48	$10.6^{+2.0}_{-0.5}$ @ 47	$-1.08^{+0.06}_{-0.04}$ @ 36	57
Zeolite GT	2019	D	508	249	34–48	−2.753	−8.00	$-1.08^{+0.05}_{-0.06}$ @ 34	$-1.08^{+0.02}_{-0.02}$ @ 38	$-1.25^{+0.15}_{-0.10}$ @ 48	$10.7^{+1.9}_{-0.6}$ @ 47	$-1.07^{+0.05}_{-0.02}$ @ 36	57
Zeolite 2 GT	2023	D	637	210	35–49	−3.095	−7.25	$-1.03^{+0.05}_{-0.07}$ @ 35	$-1.08^{+0.01}_{-0.01}$ @ 40	$-1.31^{+0.14}_{-0.09}$ @ 49	$10.6^{+1.0}_{-0.2}$ @ 44	$-1.03^{+0.05}_{-0.07}$ @ <35	58

Table 3 continued

Type	Year	Class	Flights	Days	Window	a	b	s at window start	s at most flown v	s at window end	$(L/D)_{\max}$	$s_{\min}$	MS
EN C (24 types)													
Alpina 2	2013	C	127	86	31–39	−3.447	−7.59	$-1.10^{+0.09}_{-0.09}$ @ 31	$-1.11^{+0.03}_{-0.03}$ @ 36	$-1.14^{+0.06}_{-0.05}$ @ 39	$9.5^{+0.5}_{-0.4}$ @ >39	$-1.09^{+0.09}_{-0.03}$ @ 33	52
Alpina 3	2017	C	303	173	31–39	−3.298	−7.50	$-1.08^{+0.06}_{-0.07}$ @ 31	$-1.08^{+0.02}_{-0.02}$ @ 36	$-1.11^{+0.05}_{-0.04}$ @ 39	$9.8^{+0.5}_{-0.4}$ @ >39	$-1.07^{+0.05}_{-0.02}$ @ 34	52
Alpina 4	2020	C	871	360	31–39	−2.707	−8.25	$-1.13^{+0.06}_{-0.08}$ @ 31	$-1.10^{+0.01}_{-0.01}$ @ 36	$-1.11^{+0.04}_{-0.03}$ @ 39	$9.8^{+0.4}_{-0.3}$ @ >39	$-1.10^{+0.06}_{-0.01}$ @ 36	52
Artik 6	2020	C	334	210	32–40	−3.336	−7.51	$-1.08^{+0.06}_{-0.08}$ @ 32	$-1.09^{+0.03}_{-0.02}$ @ 37	$-1.13^{+0.07}_{-0.04}$ @ 40	$9.8^{+0.7}_{-0.3}$ @ >40	$-1.08^{+0.06}_{-0.03}$ @ 34	52
Artik R	2022	C	279	162	33–41	−2.848	−7.97	$-1.09^{+0.07}_{-0.07}$ @ 33	$-1.09^{+0.03}_{-0.02}$ @ 38	$-1.12^{+0.07}_{-0.05}$ @ 41	$10.2^{+0.6}_{-0.5}$ @ >41	$-1.08^{+0.07}_{-0.02}$ @ 35	54
Artik 7 P	2024	C	299	127	33–41	−2.719	−8.13	$-1.10^{+0.05}_{-0.07}$ @ 33	$-1.09^{+0.02}_{-0.02}$ @ 38	$-1.12^{+0.06}_{-0.05}$ @ 41	$10.2^{+0.5}_{-0.4}$ @ >41	$-1.08^{+0.05}_{-0.02}$ @ 36	53
Bonanza 2	2018	C	106	93	32–40	−2.272	−8.98	$-1.17^{+0.08}_{-0.08}$ @ 32	$-1.12^{+0.03}_{-0.03}$ @ 37	$-1.12^{+0.06}_{-0.05}$ @ 40	$9.9^{+0.6}_{-0.5}$ @ >40	$-1.12^{+0.12}_{-0.03}$ @ 39	55
Bonanza 3	2023	C	109	81	33–41	−2.111	−8.83	$-1.13^{+0.08}_{-0.09}$ @ 33	$-1.08^{+0.03}_{-0.04}$ @ 38	$-1.09^{+0.06}_{-0.06}$ @ 41	$10.5^{+0.6}_{-0.6}$ @ >41	$-1.08^{+0.18}_{-0.03}$ @ 39	54
Camino	2019	C	129	99	34–42	−2.691	−9.06	$-1.19^{+0.06}_{-0.08}$ @ 34	$-1.18^{+0.03}_{-0.04}$ @ 39	$-1.20^{+0.07}_{-0.08}$ @ 42	$9.7^{+0.6}_{-0.6}$ @ >42	$-1.17^{+0.07}_{-0.03}$ @ 37	53
Cure	2015	C	106	93	32–40	−2.970	−8.56	$-1.17^{+0.10}_{-0.11}$ @ 32	$-1.16^{+0.03}_{-0.03}$ @ 37	$-1.18^{+0.07}_{-0.04}$ @ 40	$9.4^{+0.6}_{-0.3}$ @ >40	$-1.15^{+0.10}_{-0.03}$ @ 36	52
Delta 3	2017	C	183	128	32–40	−2.670	−8.61	$-1.16^{+0.07}_{-0.08}$ @ 32	$-1.13^{+0.02}_{-0.03}$ @ 37	$-1.14^{+0.05}_{-0.05}$ @ 40	$9.7^{+0.4}_{-0.4}$ @ >40	$-1.13^{+0.06}_{-0.02}$ @ 37	52
Delta 4	2020	C	416	252	33–41	−2.143	−9.06	$-1.15^{+0.06}_{-0.08}$ @ 33	$-1.11^{+0.01}_{-0.01}$ @ 38	$-1.11^{+0.06}_{-0.04}$ @ 41	$10.2^{+0.6}_{-0.3}$ @ >41	$-1.11^{+0.13}_{-0.01}$ @ 39	54
Fusion	2019	C	165	111	35–43	−2.515	−9.45	$-1.20^{+0.06}_{-0.09}$ @ 35	$-1.20^{+0.02}_{-0.03}$ @ 40	$-1.22^{+0.06}_{-0.05}$ @ 43	$9.8^{+0.5}_{-0.4}$ @ >43	$-1.19^{+0.06}_{-0.03}$ @ 38	56
Lyght	2024	C	197	105	34–42	−2.390	−8.38	$-1.09^{+0.06}_{-0.08}$ @ 34	$-1.08^{+0.02}_{-0.02}$ @ 39	$-1.10^{+0.05}_{-0.04}$ @ 42	$10.6^{+0.5}_{-0.4}$ @ >42	$-1.07^{+0.06}_{-0.02}$ @ 37	56
Lynx	2018	C	117	100	33–41	−2.598	−9.20	$-1.20^{+0.08}_{-0.08}$ @ 33	$-1.18^{+0.04}_{-0.03}$ @ 38	$-1.19^{+0.08}_{-0.06}$ @ 41	$9.6^{+0.7}_{-0.5}$ @ >41	$-1.18^{+0.11}_{-0.03}$ @ 38	52
Lynx 2	2023	C	124	91	32–40	−3.871	−7.51	$-1.12^{+0.08}_{-0.16}$ @ 32	$-1.16^{+0.05}_{-0.05}$ @ 37	$-1.21^{+0.09}_{-0.05}$ @ 40	$9.2^{+0.7}_{-0.3}$ @ >40	$-1.12^{+0.11}_{-0.08}$ @ 32	52
Photon	2023	C	589	249	34–42	−2.483	−8.42	$-1.10^{+0.05}_{-0.07}$ @ 34	$-1.09^{+0.01}_{-0.01}$ @ 39	$-1.12^{+0.05}_{-0.04}$ @ 42	$10.5^{+0.4}_{-0.4}$ @ >42	$-1.09^{+0.05}_{-0.02}$ @ 37	56
Savage	2020	C	268	169	31–39	−3.388	−7.54	$-1.09^{+0.05}_{-0.07}$ @ 31	$-1.09^{+0.02}_{-0.02}$ @ 36	$-1.13^{+0.05}_{-0.04}$ @ 39	$9.6^{+0.4}_{-0.4}$ @ >39	$-1.08^{+0.04}_{-0.02}$ @ 33	52
Sigma 7	2008	C	224	150	30–38	−3.995	−7.94	$-1.18^{+0.09}_{-0.08}$ @ 30	$-1.19^{+0.03}_{-0.02}$ @ 35	$-1.22^{+0.05}_{-0.05}$ @ 38	$8.6^{+0.4}_{-0.3}$ @ >38	$-1.17^{+0.09}_{-0.03}$ @ 32	52
Sigma 8	2010	C	239	148	31–39	−3.299	−8.40	$-1.19^{+0.06}_{-0.07}$ @ 31	$-1.17^{+0.03}_{-0.03}$ @ 36	$-1.20^{+0.06}_{-0.05}$ @ 39	$9.1^{+0.5}_{-0.4}$ @ >39	$-1.17^{+0.05}_{-0.02}$ @ 35	50
Sigma 10	2017	C	284	177	32–40	−2.921	−8.13	$-1.12^{+0.07}_{-0.06}$ @ 32	$-1.11^{+0.03}_{-0.03}$ @ 37	$-1.13^{+0.05}_{-0.06}$ @ 40	$9.8^{+0.5}_{-0.5}$ @ >40	$-1.10^{+0.06}_{-0.03}$ @ 35	52
Sigma 11	2020	C	322	196	33–41	−2.424	−9.16	$-1.19^{+0.07}_{-0.08}$ @ 33	$-1.15^{+0.02}_{-0.02}$ @ 38	$-1.16^{+0.04}_{-0.04}$ @ 41	$9.8^{+0.4}_{-0.3}$ @ >41	$-1.15^{+0.06}_{-0.02}$ @ 38	55
Sigma DLS	2024	C	148	93	33–41	−2.031	−9.73	$-1.22^{+0.05}_{-0.07}$ @ 33	$-1.16^{+0.02}_{-0.02}$ @ 38	$-1.15^{+0.05}_{-0.05}$ @ 41	$9.9^{+0.5}_{-0.4}$ @ >41	$-1.15^{+0.14}_{-0.02}$ @ 40	52
Volt 4	2022	C	367	204	31–39	−2.540	−8.34	$-1.13^{+0.05}_{-0.08}$ @ 31	$-1.09^{+0.02}_{-0.01}$ @ 36	$-1.09^{+0.05}_{-0.04}$ @ 39	$9.9^{+0.4}_{-0.3}$ @ >39	$-1.09^{+0.08}_{-0.01}$ @ 37	52
EN B (35 types)													
Arak	2018	B	267	169	32–40	−2.532	−9.37	$-1.23^{+0.04}_{-0.06}$ @ 32	$-1.19^{+0.02}_{-0.02}$ @ 36	$-1.19^{+0.09}_{-0.06}$ @ 40	$9.3^{+0.7}_{-0.4}$ @ >40	$-1.19^{+0.13}_{-0.02}$ @ 38	49
Arak Air	2021	B	339	181	31–39	−3.350	−8.44	$-1.19^{+0.05}_{-0.08}$ @ 31	$-1.18^{+0.02}_{-0.03}$ @ 35	$-1.21^{+0.07}_{-0.05}$ @ 39	$9.0^{+0.5}_{-0.4}$ @ >39	$-1.18^{+0.05}_{-0.02}$ @ 34	50
Beat Light	2021	B	145	104	32–40	−2.854	−9.53	$-1.27^{+0.09}_{-0.07}$ @ 32	$-1.24^{+0.05}_{-0.04}$ @ 35	$-1.25^{+0.07}_{-0.06}$ @ 40	$8.9^{+0.5}_{-0.4}$ @ >40	$-1.24^{+0.08}_{-0.03}$ @ 37	50
Cumeo	2018	B	156	121	33–41	−2.183	−9.24	$-1.18^{+0.05}_{-0.05}$ @ 33	$-1.14^{+0.02}_{-0.01}$ @ 37	$-1.13^{+0.07}_{-0.05}$ @ 41	$10.1^{+0.6}_{-0.5}$ @ >41	$-1.13^{+0.11}_{-0.02}$ @ 39	52
Epsilon 9	2018	B	343	239	31–39	−3.766	−8.46	$-1.22^{+0.07}_{-0.10}$ @ 31	$-1.22^{+0.04}_{-0.03}$ @ 35	$-1.26^{+0.08}_{-0.05}$ @ 39	$8.6^{+0.6}_{-0.3}$ @ >39	$-1.21^{+0.06}_{-0.03}$ @ 34	50
Epsilon DLS	2022	B	329	179	30–38	−2.583	−9.23	$-1.26^{+0.05}_{-0.07}$ @ 30	$-1.19^{+0.02}_{-0.02}$ @ 34	$-1.18^{+0.06}_{-0.04}$ @ 38	$9.0^{+0.5}_{-0.3}$ @ >38	$-1.18^{+0.12}_{-0.02}$ @ 38	48
Explorer	2017	B	254	184	32–40	−2.921	−8.46	$-1.16^{+0.04}_{-0.06}$ @ 32	$-1.14^{+0.01}_{-0.02}$ @ 36	$-1.16^{+0.07}_{-0.04}$ @ 40	$9.6^{+0.6}_{-0.3}$ @ >40	$-1.14^{+0.06}_{-0.01}$ @ 36	50
Explorer 2	2021	B	217	141	32–40	−2.325	−8.96	$-1.17^{+0.04}_{-0.06}$ @ 32	$-1.13^{+0.02}_{-0.02}$ @ 36	$-1.12^{+0.07}_{-0.05}$ @ 40	$9.9^{+0.7}_{-0.5}$ @ >40	$-1.12^{+0.11}_{-0.02}$ @ 38	50
Geo 5	2016	B	104	84	31–39	−3.862	−7.94	$-1.17^{+0.06}_{-0.07}$ @ 31	$-1.17^{+0.02}_{-0.04}$ @ 35	$-1.22^{+0.10}_{-0.08}$ @ 39	$8.9^{+0.8}_{-0.5}$ @ >39	$-1.16^{+0.06}_{-0.04}$ @ 33	50
Geo 6	2019	B	153	119	31–39	−1.586	−10.00	$-1.26^{+0.06}_{-0.08}$ @ 31	$-1.18^{+0.04}_{-0.03}$ @ 35	$-1.12^{+0.07}_{-0.05}$ @ 39	$9.6^{+0.6}_{-0.4}$ @ >39	$-1.12^{+0.07}_{-0.05}$ @ >39	50

Table 3 continued

Type	Year	Class	Flights	Days	Window	a	b	s at window start	s at most flown v	s at window end	$(L/D)_{\max}$	$s_{\min}$	MS
Ikuma 2 P	2020	B	228	148	31–39	−2.268	−8.72	$-1.16^{+0.07}_{-0.06}$ @ 31	$-1.11^{+0.03}_{-0.06}$ @ 35	$-1.09^{+0.07}_{-0.06}$ @ 39	$9.9^{+0.7}_{-0.5}$ @ >39	$-1.09^{+0.16}_{-0.03}$ @ 38	50
Ikuma 3 P	2023	B	288	145	31–39	−2.862	−8.06	$-1.12^{+0.05}_{-0.06}$ @ 31	$-1.09^{+0.02}_{-0.02}$ @ 35	$-1.11^{+0.07}_{-0.06}$ @ 39	$9.8^{+0.6}_{-0.5}$ @ >39	$-1.09^{+0.08}_{-0.01}$ @ 35	49
Ion 4	2016	B	188	133	33–41	−2.839	−9.31	$-1.23^{+0.05}_{-0.06}$ @ 33	$-1.21^{+0.02}_{-0.02}$ @ 37	$-1.24^{+0.08}_{-0.05}$ @ 41	$9.2^{+0.6}_{-0.4}$ @ >41	$-1.21^{+0.07}_{-0.02}$ @ 37	56
Iota	2014	B	624	401	33–41	−2.145	−9.58	$-1.21^{+0.04}_{-0.05}$ @ 33	$-1.17^{+0.02}_{-0.01}$ @ 36	$-1.16^{+0.07}_{-0.06}$ @ 41	$9.8^{+0.7}_{-0.4}$ @ >41	$-1.16^{+0.13}_{-0.02}$ @ 40	51
Iota 2	2017	B	412	240	32–40	−3.135	−8.08	$-1.13^{+0.05}_{-0.07}$ @ 32	$-1.12^{+0.03}_{-0.03}$ @ 36	$-1.16^{+0.08}_{-0.06}$ @ 40	$9.6^{+0.7}_{-0.5}$ @ >40	$-1.12^{+0.06}_{-0.02}$ @ 35	51
Iota DLS	2021	B	635	270	33–41	−2.575	−8.80	$-1.16^{+0.04}_{-0.05}$ @ 33	$-1.14^{+0.02}_{-0.01}$ @ 37	$-1.15^{+0.07}_{-0.05}$ @ 41	$9.9^{+0.6}_{-0.4}$ @ >41	$-1.14^{+0.07}_{-0.01}$ @ 37	52
Maestro	2019	B	154	108	33–41	−2.551	−8.52	$-1.13^{+0.06}_{-0.06}$ @ 33	$-1.11^{+0.03}_{-0.04}$ @ 36	$-1.12^{+0.09}_{-0.08}$ @ 41	$10.1^{+0.9}_{-0.7}$ @ >41	$-1.11^{+0.10}_{-0.03}$ @ 37	51
Maestro X-Alps	2019	B	203	140	32–40	−3.304	−8.54	$-1.19^{+0.06}_{-0.06}$ @ 32	$-1.19^{+0.03}_{-0.02}$ @ 36	$-1.22^{+0.07}_{-0.05}$ @ 40	$9.1^{+0.6}_{-0.4}$ @ >40	$-1.18^{+0.06}_{-0.03}$ @ 35	52
Maestro 2 Light	2022	B	179	111	32–40	−3.195	−7.87	$-1.11^{+0.06}_{-0.10}$ @ 32	$-1.11^{+0.04}_{-0.04}$ @ 36	$-1.15^{+0.08}_{-0.06}$ @ 40	$9.7^{+0.7}_{-0.4}$ @ >40	$-1.10^{+0.08}_{-0.04}$ @ 34	52
Mentor	2008	B	283	191	33–41	−2.936	−9.61	$-1.27^{+0.09}_{-0.08}$ @ 33	$-1.25^{+0.04}_{-0.03}$ @ 37	$-1.28^{+0.06}_{-0.06}$ @ 41	$8.9^{+0.5}_{-0.4}$ @ >41	$-1.25^{+0.09}_{-0.03}$ @ 37	54
Mentor 2	2010	B	259	153	32–40	−2.526	−9.07	$-1.20^{+0.05}_{-0.06}$ @ 32	$-1.16^{+0.02}_{-0.02}$ @ 36	$-1.16^{+0.07}_{-0.06}$ @ 40	$9.6^{+0.6}_{-0.4}$ @ >40	$-1.16^{+0.11}_{-0.02}$ @ 38	54
Mentor 4	2014	B	153	118	34–42	−2.527	−8.94	$-1.16^{+0.05}_{-0.06}$ @ 34	$-1.14^{+0.02}_{-0.03}$ @ 38	$-1.17^{+0.08}_{-0.05}$ @ 42	$10.0^{+0.7}_{-0.4}$ @ >42	$-1.14^{+0.07}_{-0.02}$ @ 38	55
Mentor 5	2017	B	155	111	34–42	−2.587	−9.56	$-1.23^{+0.07}_{-0.05}$ @ 34	$-1.21^{+0.03}_{-0.03}$ @ 38	$-1.23^{+0.08}_{-0.07}$ @ 42	$9.5^{+0.6}_{-0.5}$ @ >42	$-1.21^{+0.08}_{-0.02}$ @ 38	54
Mentor 5 Light	2017	B	103	76	34–42	−2.722	−9.49	$-1.23^{+0.08}_{-0.08}$ @ 34	$-1.22^{+0.04}_{-0.04}$ @ 38	$-1.25^{+0.08}_{-0.07}$ @ 42	$9.4^{+0.6}_{-0.5}$ @ >42	$-1.22^{+0.09}_{-0.03}$ @ 37	52
Mentor 7 Light	2022	B	267	168	33–41	−3.406	−7.85	$-1.12^{+0.04}_{-0.08}$ @ 33	$-1.13^{+0.02}_{-0.03}$ @ 37	$-1.19^{+0.08}_{-0.06}$ @ 41	$9.6^{+0.7}_{-0.5}$ @ >41	$-1.12^{+0.06}_{-0.04}$ @ 34	53
Phantom	2016	B	229	186	31–39	−2.812	−9.17	$-1.25^{+0.04}_{-0.06}$ @ 31	$-1.20^{+0.02}_{-0.02}$ @ 35	$-1.20^{+0.06}_{-0.05}$ @ 39	$9.0^{+0.5}_{-0.3}$ @ >39	$-1.20^{+0.10}_{-0.02}$ @ 37	50
Rush 4	2014	B	162	117	32–40	−3.022	−8.29	$-1.15^{+0.06}_{-0.07}$ @ 32	$-1.13^{+0.02}_{-0.02}$ @ 36	$-1.16^{+0.06}_{-0.05}$ @ 40	$9.6^{+0.5}_{-0.4}$ @ >40	$-1.13^{+0.05}_{-0.02}$ @ 35	52
Rush 5	2018	B	153	123	32–40	−2.480	−8.37	$-1.11^{+0.08}_{-0.07}$ @ 32	$-1.08^{+0.04}_{-0.03}$ @ 36	$-1.09^{+0.07}_{-0.05}$ @ 40	$10.2^{+0.7}_{-0.5}$ @ >40	$-1.08^{+0.10}_{-0.02}$ @ 37	51
Rush 6	2021	B	208	138	33–41	−2.184	−9.04	$-1.16^{+0.04}_{-0.07}$ @ 33	$-1.12^{+0.02}_{-0.03}$ @ 36	$-1.12^{+0.07}_{-0.06}$ @ 41	$10.2^{+0.7}_{-0.5}$ @ >41	$-1.11^{+0.16}_{-0.02}$ @ 39	50
Soar	2020	B	328	235	32–40	−2.961	−8.66	$-1.18^{+0.05}_{-0.06}$ @ 32	$-1.16^{+0.03}_{-0.02}$ @ 36	$-1.19^{+0.07}_{-0.05}$ @ 40	$9.4^{+0.6}_{-0.4}$ @ >40	$-1.16^{+0.06}_{-0.02}$ @ 36	51
Swift 4	2014	B	345	256	31–39	−3.295	−7.75	$-1.11^{+0.05}_{-0.06}$ @ 31	$-1.10^{+0.02}_{-0.02}$ @ 35	$-1.14^{+0.07}_{-0.06}$ @ 39	$9.5^{+0.6}_{-0.5}$ @ >39	$-1.10^{+0.04}_{-0.01}$ @ 34	50
Swift 5	2018	B	495	260	32–40	−2.527	−8.39	$-1.12^{+0.04}_{-0.06}$ @ 32	$-1.09^{+0.02}_{-0.02}$ @ 36	$-1.10^{+0.06}_{-0.05}$ @ 40	$10.1^{+0.6}_{-0.5}$ @ >40	$-1.09^{+0.07}_{-0.01}$ @ 37	51
Swift 6	2022	B	594	262	32–40	−2.811	−8.23	$-1.12^{+0.05}_{-0.06}$ @ 32	$-1.10^{+0.01}_{-0.01}$ @ 36	$-1.13^{+0.06}_{-0.04}$ @ 40	$9.9^{+0.6}_{-0.4}$ @ >40	$-1.10^{+0.05}_{-0.01}$ @ 36	54
Tenor Light	2018	B	148	121	31–39	−3.576	−8.77	$-1.25^{+0.05}_{-0.08}$ @ 31	$-1.23^{+0.03}_{-0.03}$ @ 35	$-1.26^{+0.07}_{-0.05}$ @ 39	$8.6^{+0.5}_{-0.3}$ @ >39	$-1.23^{+0.05}_{-0.03}$ @ 34	50
Xi	2018	B	634	335	32–40	−2.508	−8.87	$-1.17^{+0.04}_{-0.06}$ @ 32	$-1.14^{+0.02}_{-0.02}$ @ 36	$-1.14^{+0.07}_{-0.05}$ @ 40	$9.7^{+0.6}_{-0.4}$ @ >40	$-1.14^{+0.10}_{-0.01}$ @ 38	52
EN A (1 type)													
Koyot 3	2016	A	116	97	29–37	−4.172	−9.15	$-1.35^{+0.07}_{-0.10}$ @ 29	$-1.32^{+0.02}_{-0.03}$ @ 35	$-1.34^{+0.05}_{-0.04}$ @ 37	$7.6^{+0.3}_{-0.2}$ @ >37	$-1.32^{+0.05}_{-0.03}$ @ 33	46
Class and periods (Sections 4.1 and 4.4)													
EN D class (all types)	–	D	5096	1043	34–48	−2.574	−8.04	$-1.07^{+0.04}_{-0.06}$ @ 34	$-1.07^{+0.01}_{-0.01}$ @ 39	$-1.21^{+0.13}_{-0.10}$ @ 48	$11.0^{+1.8}_{-0.6}$ @ 48	$-1.06^{+0.04}_{-0.01}$ @ 36	57
EN D class, to 2023	–	D	2946	731	34–48	−2.507	−8.28	$-1.09^{+0.04}_{-0.05}$ @ 34	$-1.08^{+0.01}_{-0.01}$ @ 39	$-1.22^{+0.13}_{-0.09}$ @ 48	$11.0^{+1.3}_{-0.8}$ @ >48	$-1.08^{+0.03}_{-0.01}$ @ 37	56
EN D class, from 2024	–	D	2150	312	34–48	−2.685	−7.69	$-1.04^{+0.04}_{-0.06}$ @ 34	$-1.05^{+0.01}_{-0.01}$ @ 39	$-1.21^{+0.13}_{-0.09}$ @ 48	$11.0^{+1.6}_{-0.5}$ @ 47	$-1.04^{+0.04}_{-0.02}$ @ 36	58
Enzo 3, to 2023	–	CCC	435	191	34–51	−2.620	−7.39	$-1.00^{+0.06}_{-0.08}$ @ 34	$-1.03^{+0.01}_{-0.01}$ @ 41	$-1.27^{+0.15}_{-0.11}$ @ 51	$11.4^{+1.3}_{-0.4}$ @ 47	$-1.00^{+0.06}_{-0.04}$ @ 35	61
Enzo 3, from 2024	–	CCC	155	72	34–51	−2.258	−7.39	$-0.97^{+0.06}_{-0.09}$ @ 34	$-0.98^{+0.02}_{-0.03}$ @ 41	$-1.16^{+0.15}_{-0.10}$ @ 51	$12.2^{+2.2}_{-0.6}$ @ 48	$-0.96^{+0.05}_{-0.04}$ @ 37	62

Table 3 continued

Type	Year	Class	Flights	Days	Window	a	b	s at window start	s at most flown v	s at window end	$(L/D)_{max}$	s_{min}	MS

Without polar: Alpha 5 (one pilot, 41 % of the flights); Apollo 2 (one pilot, 36 % of the flights); Aya (one pilot, 47 % of the flights); Base 2 (one pilot, 50 % of the flights); Beat (one pilot, 64 % of the flights); Chili 5 (polar changes by 0.04 m s^{-1} at 36 km h^{-1} without the pilot with the most flights, 20 %); Epsilon 6 (one pilot, 31 % of the flights); Epsilon 7 (polar changes by 0.03 m s^{-1} at 34 km h^{-1} without the pilot with the most flights, 27 %); Epsilon 8 (one pilot, 34 % of the flights); Factor 2 (one pilot, 41 % of the flights); Hook 5 P (one pilot, 46 % of the flights); Hook 6 P (one pilot, 57 % of the flights); Ikuma 2 (too few seconds in the window); Ikuma 3 (one pilot, 45 % of the flights); Ion 6 Light (one pilot, 40 % of the flights); Klimber 2 P (one pilot, 45 % of the flights); Klimber 3 P (one pilot, 42 % of the flights); Klimber P (one pilot, 43 % of the flights); LM 6 (points do not follow the physical curve); LM 7 (one pilot, 53 % of the flights); Mentor 3 (points do not follow the physical curve); Mistral 4 (one pilot, 36 % of the flights); Mojo 6 (points do not follow the physical curve); Peak 3 (one pilot, 57 % of the flights); Pi 2 (one pilot, 43 % of the flights); Pi 3 (one pilot, 54 % of the flights); Sigma 6 (points do not follow the physical curve); Sigma 9 (one pilot, 42 % of the flights); Susi 3 (one pilot, 33 % of the flights); Swift (one pilot, 42 % of the flights); Symphonia (one pilot, 69 % of the flights); Theta ULS (polar changes by 0.06 m s^{-1} at 41 km h^{-1} without the pilot with the most flights, 17 %); Volt 3 (one pilot, 70 % of the flights).

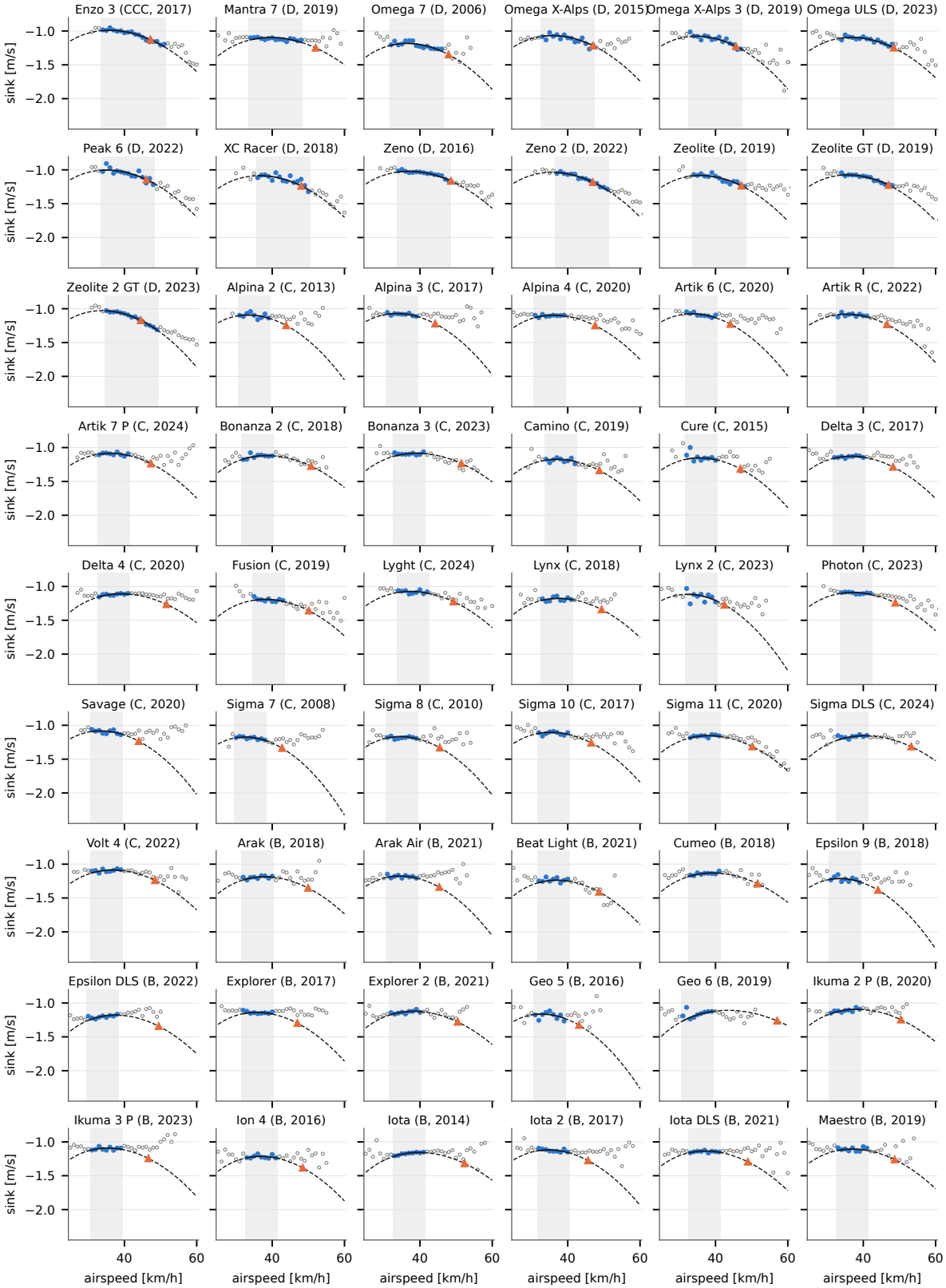

Figure 16: Polars of the glider types of Table 3, in the order of the table (part 1; part 2 in Figure 17). Points: most frequent value in 1 km h^{-1} bands at 2000 m after the corrections for subsidence and for the choice of speed; filled in the window of the type (shaded), open outside. Line: the physical curve fitted in the window, dashed outside. Triangle: best glide ratio of the curve. In brackets: class and year.

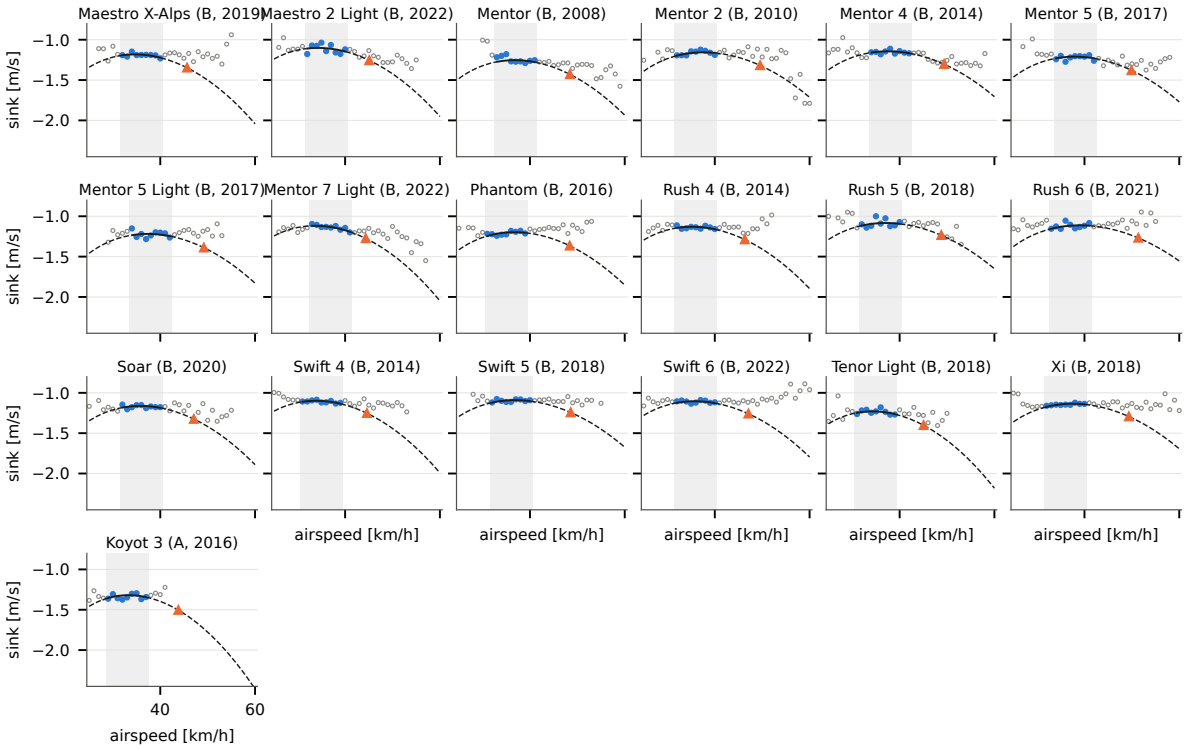

Figure 17: Polars of the glider types of Table 3, part 2; as in Figure 16.